NTNU

Norwegian University of
Science and Technology

Conductivity Measurement in Switching Arcs using Electric Probes

Torjus Ramm Settendal

Master of Energy Use and Energy Planning
Submission date: June 2017
Supervisor: Kaveh Niayesh, IEL

Norwegian University of Science and Technology
Department of Electric Power Engineering

Preface

This thesis is submitted as the primary evaluation criterion for the course TET4910, and partial requirement for the Msc course Energy Use and Planning at the Norwegian University of Science and Technology (NTNU). The work presented here has been performed in collaboration with PhD candidate Henning Taxt, and is based on his current work. This work is a continuation of the authors previous work conducted as part of the specialization project (TET4510).

June 11, 2017

Torjus Ramm Settendal

Acknowledgments

Foremost, I would like to thank my supervisor Professor Kaveh Niayesh for his invaluable insight, guidance, and support. I would also like to thank Henning Taxt for committing his time to both educate and support me, be it in the lab or in writing this thesis. Finally, I would like to thank the support staff in the service lab and workshops at NTNU for providing and procuring the equipment used in this work.

Trondheim, June 2017

Torjus Ramm Settendal

Abstract

Due to its excellent arc quenching capability, SF_6-gas is widely used for medium voltage switchgear. Because it is a highly potent greenhouse gas, it is expected to be many restrictions for the allowed use of this gas in near future. It is therefore important to conduct research on development of more environmental friendly switchgear. The challenge is to keep both the interruption capability and volume, of todays SF_6 insulated switchgear. One of the most promising solution to this challenge, is to use ablation material to improve the current interruption capability. Experimental work with an ablation-assisted circuit breaker, is the foundation for the work in this thesis.

The primary aim of this thesis is to evaluate the arc voltage distribution inside an ablation tube during ablation-assisted current interruption, using air as the insulation medium. This is performed by gathering the readouts from three high voltage resistive probes placed at different key locations in the plasma arc.

The first part of the thesis contains work performed to weed out any large sources of measurement error. From previous work, it was found that the experimental setup used in this work contained one or more of these sources. The second part of this work contains the experimental portion of this work. This part explains how the tests were conducted, and lists the results together with a discussion around their significance and wider implications.

By applying the corrections suggested in this work, the probes gave valuable results for conductivity measurements in switching arcs. The results are considered valid for measurements from contact separation and until 100 μs after current interruption.

The results show clearly that the field strength was significantly higher where the gas outlet was located, when the pressure inside the ablation tube was low. When acting as a "self-blast" switch, which increased the pressure, gave the system an increase in field strength. Additionally, there was also a change in the position of the field strength peaks. With an increase in pressure, the field strength changed from being largest over the gas outlet to being largest over the first few millimeters of the arc.

Sammendrag

På grunn av sin utmerkede slukkeevne er SF_6 gass mye brukt for mellomspenningsbrytere. Fordi det er en betydelig drivhusgass, forventes det å komme mange restriksjoner for tillatt bruk av denne gassen i nær fremtid. Det er derfor viktig å gjøre forskning på utvikling av mer miljøvennlige bryteranlegg. Utfordringen er å beholde både bryteevnen og størrelsen til dagens SF_6 isolerte bryteranlegg. En av de mest lovende løsningene på denne utfordringen er å bruke ablasjonsmateriale for å øke bryteevnen. Forsøk med en ablasjonsassistert bryter, er grunnlaget for arbeidet i denne oppgaven.

Hovedformålet med denne oppgaven er å evaluere spenningsfordelingen til lysbuen inne i et ablasjonsrør under ablasjonsassistert bryting ved bruk av luft som isolasjonsmedium. Dette utføres ved å samle målinger fra tre resistive høyspenningsprober plassert på forskjellige nøkkelpunkter i lysbuen.

Den første delen av avhandlingen inneholder arbeid utført for å utrydde eventuelle store kilder til målefeil. Fra tidligere arbeid ble det funnet at det eksperimentelle oppsettet som ble brukt i dette arbeidet inneholdt en eller flere feilkilder. Den andre delen av dette arbeidet inneholder den eksperimentelle delen av dette arbeidet. Denne delen forklarer hvordan testene ble utført, og lister opp resultatene sammen med en diskusjon om deres betydning og bredere implikasjoner.

Ved å anvende de korreksjonene som ble foreslått i dette arbeidet ga probene verdifulle resultater for konduktivitetsmålinger i lysbuer. Resultatene anses å være gyldige for målinger fra kontaktseparering og til 100 μs etter nullgjennomgang.

Resultatene viste tydelig at feltstyrken var betydelig høyere der gassutløpet var plassert, når trykket i ablasjonsrøret var lavt. Når bryteren fungerte som en "selv blåse" bryter, gav systemet også en økning i feltstyrke. I tillegg var det også en endring i posisjonen til feltstyrketoppene. Med en økning i trykk, skiftet feltstyrken fra å være størst over gassutløpet til å være størst over de første få millimeterne av lysbuen.

Contents

Explanation of terms

Terms that are used in the thesis:

Ablation Removal of material from the surface of an object by vaporization, chipping, or other erosive processes.

amu atomic mass unit, 1 $amu \approx 1.660 \cdot 10^{-27} kg$.

CZ Current zero, refers to when the arc is extinguished and no current is flowing through the arc gap.

Homogenous Consisting of parts that are the same; uniform in structure or composition.

Diatomic molecules Molocules with only two atoms.

Isotropic Identical in all directions; invariant with respect to direction.

Mean free path The average distance that a particle travels between successive collisions with other particles.

Particle flux The rate of transfer of particles through a unit area.

SF_6 Sulfur hexafluoride.

List of Figures

List of Tables

Chapter 1

Introduction

1.1 Background and Objectives

Among the greatest challenges in the world today is climate change. As an effort to slow down heating of the earth, regulations on emissions of greenhouse gases are currently being implemented.

SF_6 has proven to be an excellent insulating medium for load break switches, however it is also a highly potent greenhouse gas. It is therefore expected that, in near future, stricter rules and regulations will be implemented to limit its use. Research is therefore being conducted on developing circuit breakers which can use environmental friendly gases, such as air, as an insulating medium.

The challenge with using air instead of SF_6 is that the switchgear needs to encompass a greater volume than one containing SF_6. Due to this, research is currently being conducted to explore new equipment designs which can utilize air without requiring a drastically increase in volume.

This report is a continuation of the specialization project that was written in the autumn semester of 2016 [3]. In this project, it was found that the method of using high voltage resistive probes to measure voltage in an ablation tube, could give valuable results. Though, the resulting voltage plots had some errors, that needed to be addressed. How they can be solved or corrected, are looked at in this thesis.

The main objectives for this thesis are:

- To determine the feasibility of utilizing high voltage resistive probes as a viable method for conductivity measurement in switching arcs.
- To determine the voltage distribution of the plasma arc inside the ablation tube of the circuit breaker.

1.2 Structure of the Thesis

This master thesis is divided into six chapters. Chapter 2 explains the basics of current interruption. An overview of the experimental work and a description of the experimental setup is given in Chapter 3. Chapter 4 investigates the reason behind the experimental errors found in the specialization project, and how to correct for it. A presentation and discussion of the results can be found in Chapter 5. In Chapter 6, the findings are summarized, the main conclusions are presented and recommendations for future work are given.

Chapter 2

Current Interruption Physics

To understand the phenomena occurring in ablation-assisted medium voltage switchgear it is important to understand the systems components, their interaction, and the underlying physics. This chapter primarily concerns itself with the two main parts of the system, namely the plasma arc and the ablation material. A brief introduction of these topics will be presented in this chapter.

2.1 Introduction

Plasma is a mixture of electrons, neutral particles and both positive and negative ions. Plasma is per definition an ionized gas that fulfills the quasi-neutral condition. This means that the density of positively and negatively charged particles in the gas, are approximately equal [3, 1, 4].

Ablation materials utilize the high temperature in the arc to enhance the current interruption capabilities of the switch. These are materials that evaporate to gases due to the high temperate, this changes the properties of the arcing medium in a beneficial matter and thus makes the current interruption easier.

2.2 Quasi-neutrality

If a plasma it subjected to outer disturbances, it can lead to a phenomena called charge separation. An example of this is when an electron is displaced too far away from its positively charged companion ion. This local charge imbalance then produces an electric field which tries to counteract the imbalance and restore the phase to its disturbed state. If we still consider the case with electrons and ions, with a charge of $-e$ and Ze respectively, the charge density can then be expressed as $(-e \cdot n_e + e \cdot Zn_i)$.

If $n_e \neq Zn_i$, there will be a space charge present and the resulting field will try to counteract the buildup of this charge. The resulting effects from this electric field are so large that the difference in the electron and ion charge densities must be as small as possible to avoid this. On small scales the electric field and potential drop might not be large enough to restore quasi-neutrality, by affecting the particle motion. The characteristic scale where charge separation can occur is known as the Debye length [3, 1, 4].

2.3 Debye Shielding

For the Debye length, the quasi-neutral condition is fulfilled. Because of a plasmas high conductivity, external electric fields are shielded from the plasmas internal effects impacting their behavior.

If one considers a case where the plasma density is N_0 and the plasma is initially electrically neutral. It is also assumed that an electrical field disturbs the plasma equilibrium state by immersing the transparent shield that has a negative potential (Φ), relative to the plasma, see Fig. 2.1. Then it can be assumed that the ion density is constant over the whole phase, and that the energy fluctuation is small relative to the temperature. Then the Debye length can be expressed as:

$$\lambda_D = \left(\frac{\epsilon_0 k T_e}{e^2 N_0} \right)^{1/2} \tag{2.1}$$

Where k is the Boltzmann constant, T_e is the electron temperature, e is the elementary charge and ϵ_0 is the permittivity of vacuum [3, 1].

The Debye length is generally small for laboratory plasmas [5]. Therefore, it can be assumed that the Debye length is much smaller than the probes characteristic dimensions.

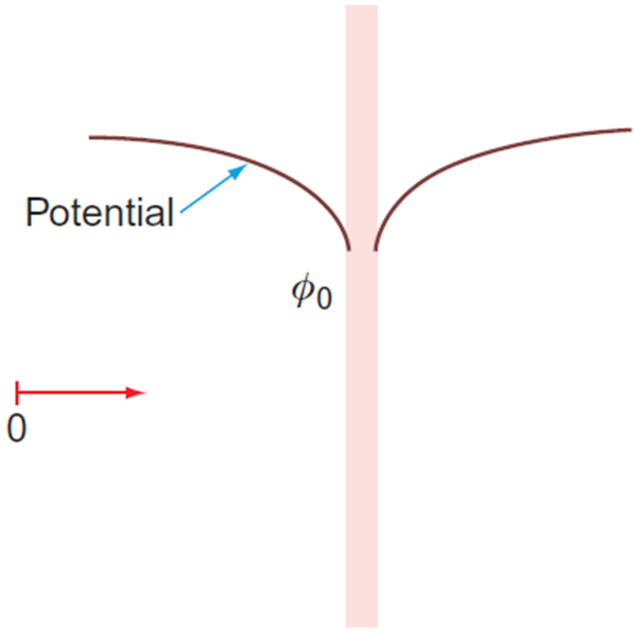

Figure 2.1: The Debye length and electric potential relative to the plasma (pink rectangle) [1].

2.4 Particle Flux

When conducting measurements on plasmas using probes it is important to understand of how the probes affect the plasma locally. In addition, one must also consider how the local parameters relate to the undisturbed plasma far away from the probe. If a plasma is isotropic and homogeneous, the particle flux density can be expressed as:

$$\Gamma = \frac{1}{4} n \overline{v} \tag{2.2}$$

Where $\overline{v}$ is the mean particle velocity and n is the particle density. The equation describes the number of particles crossing a unit area per unit time, from one side.

If a probe is inserted into a plasma where the electron and ion temperatures are similar, the mean ion velocity will be much lower than the mean electron velocity due to their relative difference in mass. Based on this, an equation for the total electric current from a probe can be described as:

$$I = -eA(\frac{1}{4}n_i\overline{v}_i - \frac{1}{4}n_e\overline{v_e}) \approx \frac{1}{4}eAn_e\overline{v}_e > 0 \tag{2.3}$$

Where e is the elementary charge, A is the probe area, n_e is the number of electrons and $\overline{v}_e$ is the mean electron velocity. A simplification is applied due to $\overline{v}_i << \overline{v}_e$. Reviewing this, it is clear that the probe will emit a net positive current [3, 5].

2.5 Collision Effects

Whether the collision effects can be neglected will strongly affect the behavior of the probe. For instance, collisions will cause a drop in the probes measured current. This is attributed to the fact that particle scattering leads to fewer particles interacting with the probe. If the plasma around the probe is treated as continuous with diffusion coefficient D, the particle current density of a perfectly absorbing spherical probe can be written as:

$$\Gamma = \frac{1}{4}n_\infty\overline{v}\frac{1}{1+\overline{v}a/4D} \tag{2.4}$$

If the effect of the electric field on particle transport is ignored and D is assumed to be constant. n_∞ is here the current density far away from the probe and a is the probe radius.

The relation between the diffusion coefficient and the mean free path can be expressed as:

$$l = \frac{3D}{\overline{v}} \tag{2.5}$$

From this, it can be concluded that the factor for drawn current is less than the random current ($\frac{1}{4}n_\infty\overline{v}$) and can be expressed as $(1+\frac{3a}{4l})^{-1}$. When $\frac{a}{l}$ is large the expression can be approximated to $\frac{4l}{3a}$. This means that for spherical probes where $l >> a$, collisions can be ignored. For cylindrical probes, it is the finite length of the probe that is the most important parameter regarding the determination of the diffusive collection. Therefore, the length of the probe should be compared to l, to determine whether or not collisions needs to be taken into consideration [3, 5].

2.6 Ablation Material Physics

The ablation material is often made into a cylinder which surrounds the electrode inside of the switch. There will be an un-ionized layer of ablation vapor between the inner surface of the tube and the plasma. The two regions, the plasma and the vapor, can be considered to have constant temperature. Only at the interface between the plasma-vapor and vapor-surface regions will there be steep temperature gradients present.

The stationary conditions of ablation-dominated arcs can be described by the conservation of energy, mass and momentum. According to the conservation of energy, the ohmic power dissipated in the arc must be equal to the expelled power. The ablation vapors' mass flux must be equal to the axial mass flux exiting the tube. Both the added mass and the ohmic heath introduced by the arc lead to an increase in pressure inside the tube, which acts as the source of momentum outward from the stagnation point. If the ease of flow is equal with respect to the axial direction, the stagnation point will be located at the center of the tube. The main challenge to exploit ablation-assisted current interruption is the slow dielectric recovery in the presence of ablation materials [6].

Chapter 3

Experimental Setup

In this chapter, the different components and setup of the test circuit used in the lab are presented. All the experiments were done at the "High Current Breaking" laboratory at NTNU.

3.1 Test Circuit at Laboratory

An overview of the test circuit is shown in Fig. 3.1. One can see that the main parts are the source side with a 6.9 kV input, the switch where the plasma arc is induced, the load side and the measuring circuit consisting of the probes. The applied current is 100 A. In addition, there are components for current measurements which are not shown in the figure.

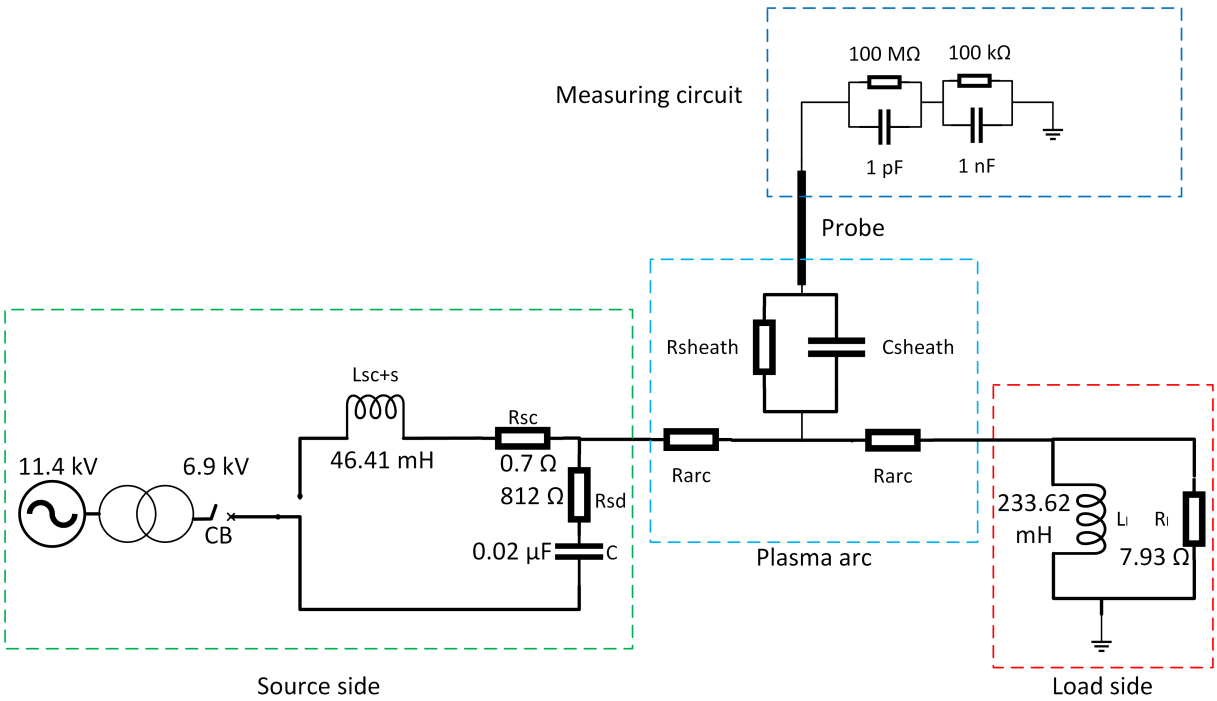

Figure 3.1: A representation of the different components in the laboratory setup. Only one probe is drawn.

3.1.1 Measuring the Current

To measure the current through the switch, two different sensors are used. One measures the high-current region and the other measures the current close to current zero crossing. Different sensors are used since it is not practical to measure both regions with the same sensor, since you need a sensor which is more sensitive with respect to lower currents in the CZ area where the currents are small [3, 7].

3.1.2 Measuring the Voltages

When conducting the experiments, high voltage electric probes were used for the measurements. The probes have an input resistance of 1 MΩ (± 1 %) and a 1000:1 ratio. Signals from the probes are transferred via fiber optic cables to a separate control room. The placement of the probes can be seen in Fig. 3.2.

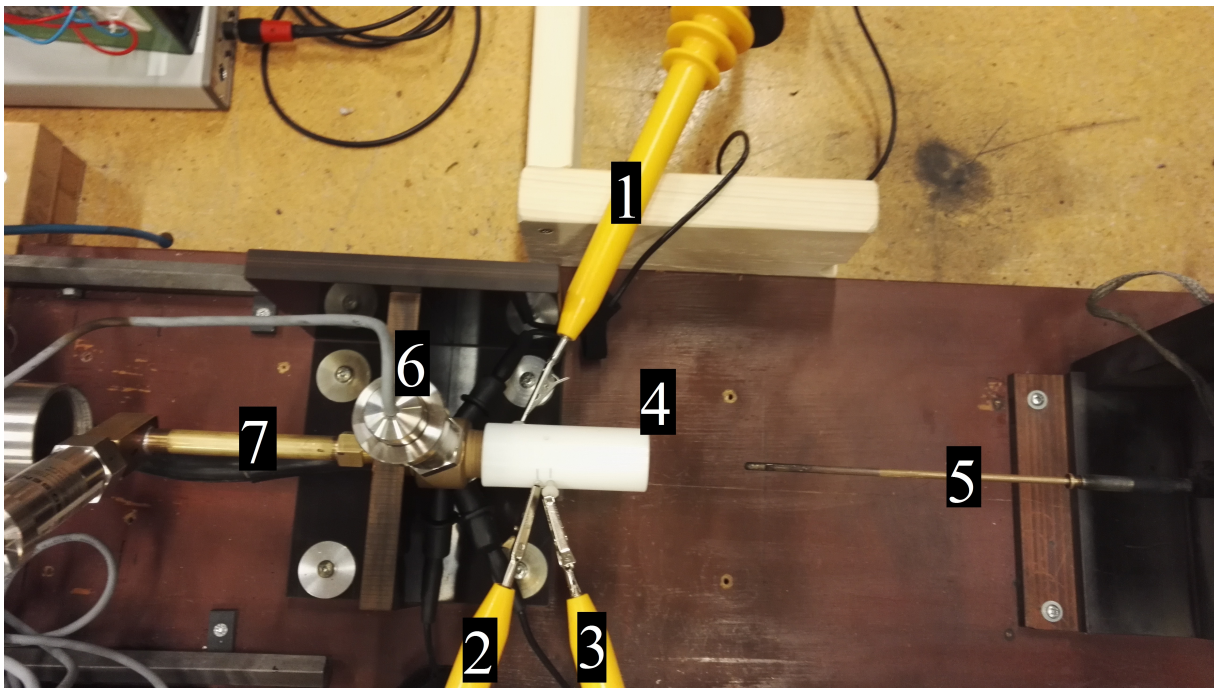

Figure 3.2: The different components are as follows:
1), 2) and **3)** Probe 1, 2 and 3.
4) Ablation tube.
5) Moving electrode.
6) Pressure measuring.
7) When mounted the switch acts as a "self-blast" switch.

3.2 Test Object

To interrupt the current, an electrode moves in the horizontal direction and an arc is ignited inside the ablation tube. The electrode will be retracted from the tube as shown in Fig. 3.3.

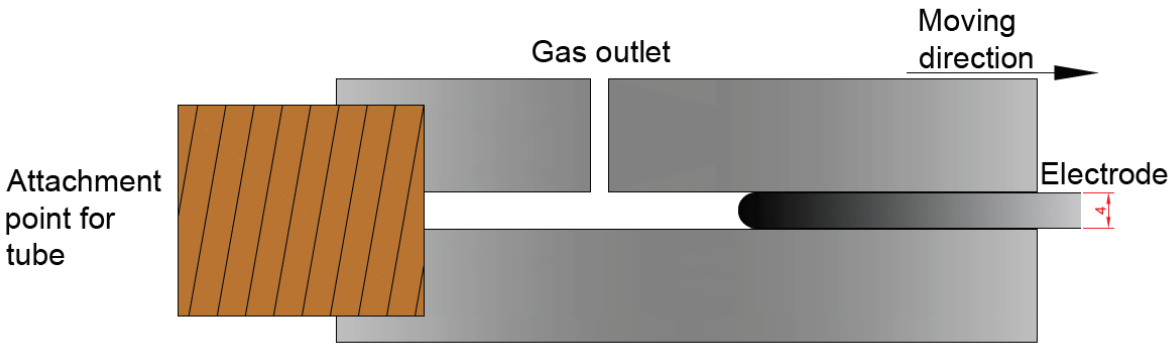

Figure 3.3: The ablation tube and the different components. The electrode moves from left to right.

In Fig. 3.2, the electrode is not charged. Before the test is conducted the electrode is moved to the left and is placed inside the ablation tube. The electrode is held in place by a charged spring connected to an electromagnet. Turning off the electromagnet releases the electrode and this can be conducted in the exact same manner every time. There is also a linear potentiometer which measures the movement [7]. When the gas flow is closed off on the left side, see number 7 in the figure, the switch acts as a type of "self-blast" switch. This stops the gases from exiting out on the left side and thus the pressure builds up. The pressure increase enhances the current interruption effect. Test were also conducted without the probes connected to the apparatus. In this case, they were positioned in such a manner that they only were in contact with the outer tube wall.

3.2.1 The Ablation Tube

The ablation material used is Polystone® Homopolymer. A drawing of the tube with dimensions is shown in Fig. 3.4a, the tube is made as a cylinder. Three holes were drilled into the tube to allow tungsten thread to be inserted for measuring purposes, see Fig. 3.5. The three holes can be seen in the middle of Fig. 3.4a. One of the holes was placed close to

the connection point (were the tube was fastened). The other two holes were placed just before and after the gas outlet where the hot gases are leaving the tube. This was done since it was deemed interesting to observe how the arc voltage distributes close to the outlet. The tungsten threads had a diameter of 0.25 mm. The thread goes through the middle of the screw and back in a hole 1 mm further down, as shown in Fig. 3.4b.

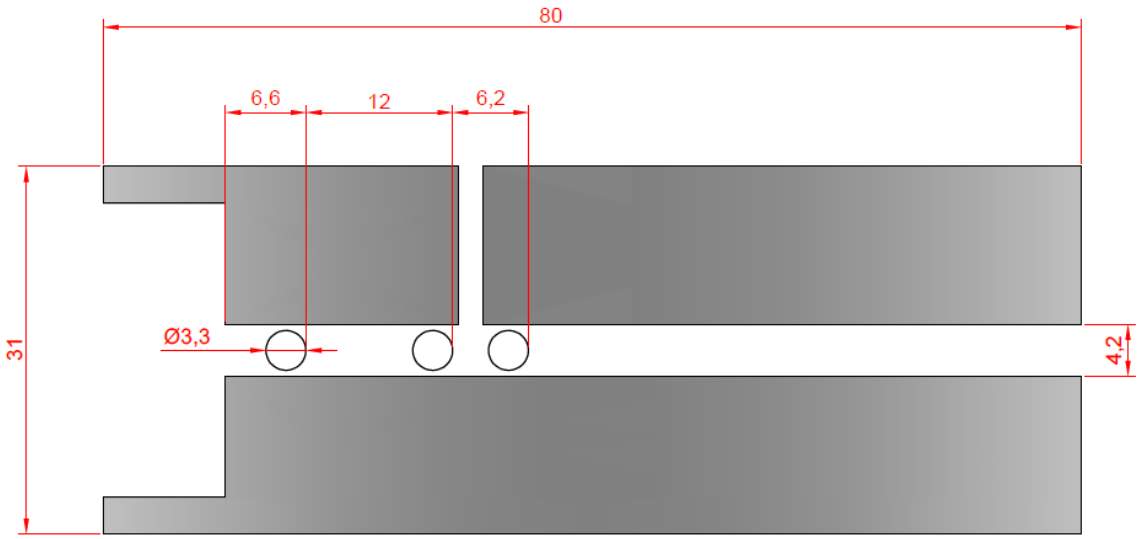

(a) Drawing of the ablation tube for the 4.0 mm electrode. The tube is identical for the 6.0 mm electrode except for the diameter of the hole for the electrode. The probes are pinched onto the wire which goes through the three horizontal holes.

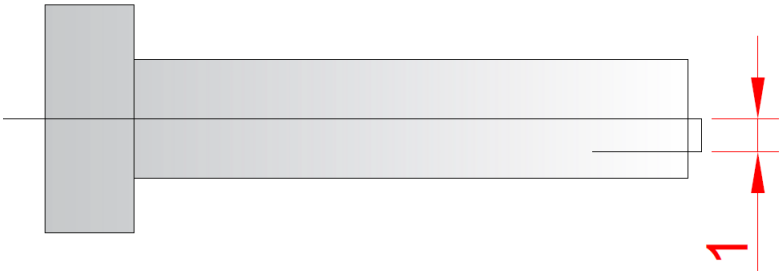

(b) The tungsten thread goes through the middle of the screw and back, to ensure an equal area for each test. The thread does not stick out as much as in the figure, this is just to illustrate. The thread is mounted so that it aligns with the sliding direction of the electrode.

Figure 3.4: Drawings of ablation tube and screw (measurements in mm).

The ablation tube works by removing some of the material, due to the heath emitted in the switching process. This leads to development of hydrogen gas which cools down the arc and thus reduces the arc conductivity and improves the arc-quenching properties. Some of the advantages using ablation is that the material is self-adjusting, as the current rises the ablation effect also rises. The downside of using ablation material is that since some of the material is burned off in each switching operation, there is a limit to how many operations

the switch can do before the material must be replaced [6].

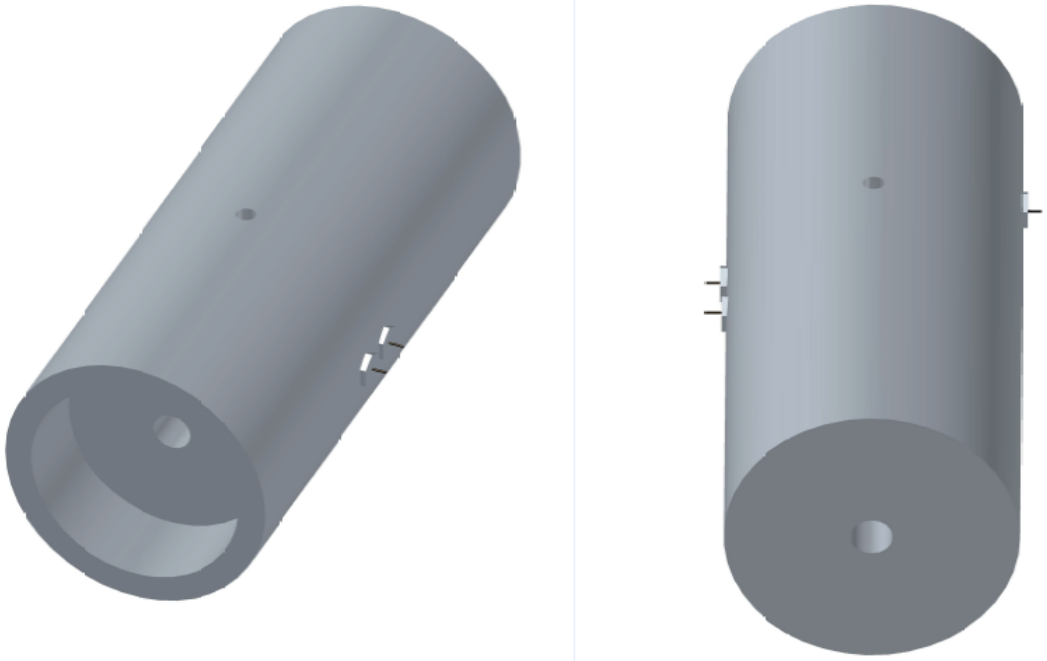

Figure 3.5: 3D model of the ablation tube. Two connections for the wire on one side, and one on the opposite side.

Chapter 4

Source of Voltage Measurement Errors

An anomaly was discovered in the earlier work by this author. It is expected that the voltages will cross zero at the same time. As this was not the case it is important to investigate why, so this error can be weeded out and corrected.

4.1 Voltage Drop in Debye Sheath

Initially it was presumed that the displacement of the voltage profiles was due to the shielding effect between the plasma and the probes. This is an effect which occurs at the probe tips, as they are submerged in the plasma. Between the bulk plasma and the electrode there will be a "shield" often called the *Debye Sheath*, see Fig. 4.1. This leads to a drop in the potential [8]. The floating potential can be expressed as:

$$V_f = V_P + \left(\frac{k_B T_e}{e}\right) \ln\left(0.6\sqrt{\frac{2\pi m_e}{m_i}}\right) \tag{4.1}$$

Where V_P is the plasma potential, k_B is the Boltzmann constant, T_e is electron temperature, e is the elementary charge, m_e and m_i represent the electron and ion masses respectively. u is the atomic unit mass.

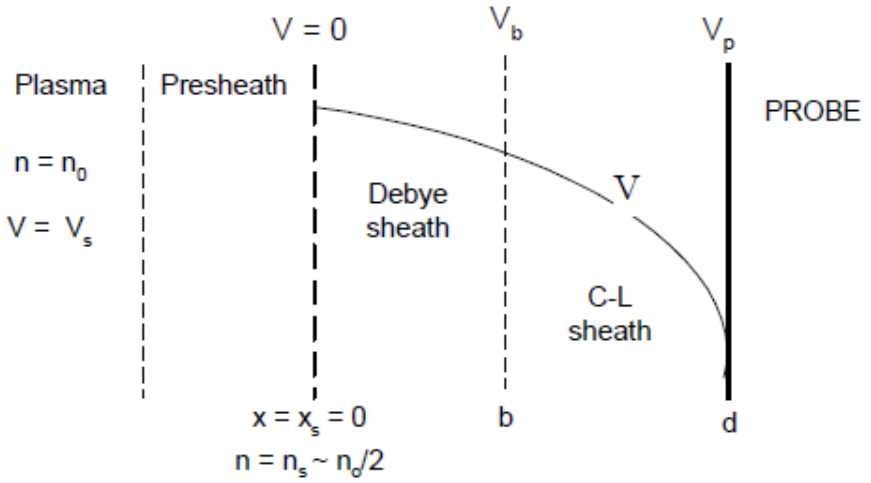

Figure 4.1: The different sheaths surrounding a probe in plasma [2].

4.1.1 Reduced Mass

It is difficult to calculate the ion mass in (4.1). Instead it is customary to use the reduced ion mass, which is defined as the mass of the ion divided by the electron mass, $\mu_i = m_i/m_e$. The total volume of air consists of about 78 % Nitrogen, 21 % Oxygen and 1 % Hydrogen. Since these are diatomic molecules, their reduced masses can be expressed as:

$$\mu = \frac{m_1 m_2}{m_1 + m_2} \tag{4.2}$$

Where m_1 and m_2 represents the mass of each of two atoms respectively. The reduced mass for the three molecules are calculated below [9].

N_2**:**

$$\mu_{N_2} = \frac{m_N m_N}{m_N + m_N} = \frac{m_N}{2} = \frac{14}{2} amu \cdot (1.660 \cdot 10^{-27} \frac{kg}{amu}) = 1.162 \cdot 10^{-26} kg$$

O_2**:**

$$\mu_{O_2} = \frac{m_O m_O}{m_O + m_O} = \frac{m_O}{2} = \frac{16}{2} amu \cdot (1.660 \cdot 10^{-27} \frac{kg}{amu}) = 1.328 \cdot 10^{-26} kg$$

H_2**:**

$$\mu_{H_2} = \frac{m_H m_H}{m_H + m_H} = \frac{m_H}{2} = \frac{1}{2} amu \cdot (1.660 \cdot 10^{-27} \frac{kg}{amu}) = 8.2 \cdot 10^{-28} kg$$

The total reduced mass of the gaseous mixture can then be calculated by adding together all the components reduced masses and weighting them by their respective mass fractions:

$$\mu_{total} = 0.78 \cdot \mu_{N_2} + 0.21 \cdot \mu_{O_2} + 0.01 \cdot \mu_{H_2}$$

$$= \left(9.064 \cdot 10^{-27} + 2.440 \cdot 10^{-27} + 8.200 \cdot 10^{-30}\right) kg$$

$$= 1.151 \cdot 10^{-26} kg$$

The last part of (4.1) can now be solved by using the reduced mass. This is then the voltage drop in the sheath (δV). This allows one to express the voltage drop present in the sheath as:

$$\delta V = \left(\frac{k_B T_e}{e}\right) \ln\left(0.6\sqrt{\frac{2\pi}{\mu_{total}}}\right) \tag{4.3}$$

4.1.2 Child-Langmuir Sheath

According to Chen [10], there will only be a Child-Langmuir Sheath if the probe is biased at a large negative voltage compared to the electron temperature. This is the sheath between the Debye sheath and the probe, see Fig. 4.1. For the experiments conducted in this thesis, it is assumed that the difference is small enough to neglect this sheath.

4.2 Simulink Model

To get a better understanding of how the Debye sheath affects the system, a model was constructed in Simulink. The model was based on the laboratory circuit, shown in Fig. 3.1.

The Simulink model can be found in Appendix A, Fig. A.1. In the model the plasma arc is represented by a series of resistances, and the probes consists of a high voltage and low voltage part, which in turn consists of a capacitance and resistance wired in parallel.

The arc resistance values used in the model are from Settendal [3], and can be seen in Table 4.1. "Test I" refers to the test conducted by Settendal, and the resistance values are calculated based on measurements from the same work.

The voltage drop in the Debye shield is represented as a constant DC voltage source, using (4.3) results in a voltage drop of 30.26 V.

Table 4.1: Arc resistances used in the Simulink circuits. The resistances are calculated using the measured voltages and applied current from previous work.

Resistance [Ω]	R1	R2	R3	R4
Test I	5.0	23.0	4.0	3.5

The following plots are generated used the earlier mentioned Simulink model. Probe 1 will always be representing the leftmost probe in the circuit, followed by probe 2 and 3. The black, blue, and red lines show the currents measured by Probe 1, 2, and 3 respectively.

Fig. 4.2 and 4.3 show the results of the first simulation, with and without the sheath present.

As seen, the graphs do not show any large deviations from each other, which indicates that the sheath has no impact on the probe currents.

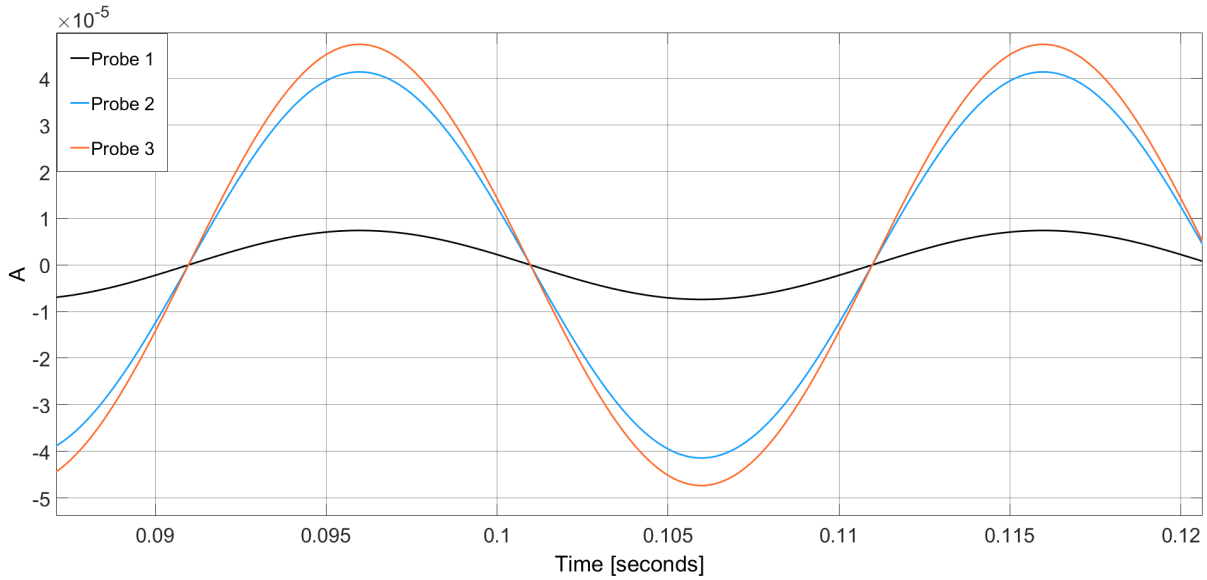

Figure 4.2: Test I: Probe currents versus time, circuit without voltage drop in sheath.

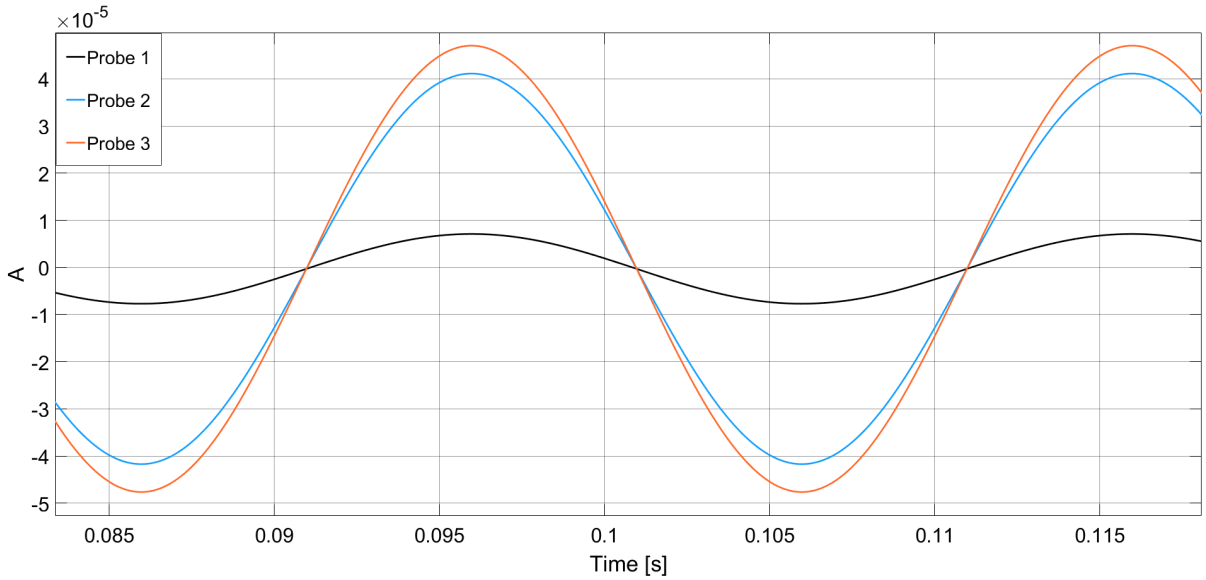

Figure 4.3: Test I: Probe currents versus time, circuit with voltage drop in sheath.

The amplitude values for the currents running through the low voltage part of the probes, are shown in Table 4.2. As previously noted, they are almost identical with just a small deviation present in the first probe. The currents are quite small and should not have any significant impact on the probes, if the current running through the switch is much larger.

Table 4.2: Simulated currents, amplitude values for low voltage part of probes. Test I

Probe	1	2	3
With voltage drop: Current [μA]	7.4	41	47
Without voltage drop: Current [μA]	7.1	41	47

The voltages for the three probes are shown in Fig. 4.4 and 4.5. Again, there is little indication that the profiles differ significantly. However, the sheath may only have an impact close to zero crossing. In Fig. 4.6 and 4.7 the view is zoomed in to where the curves cross zero. The voltages clearly do not cross at the same time, but the sheath does not seem to have any impact. Thus, the simulated voltages and currents are shifted due to the amplitude differences caused by the different arc resistance values.

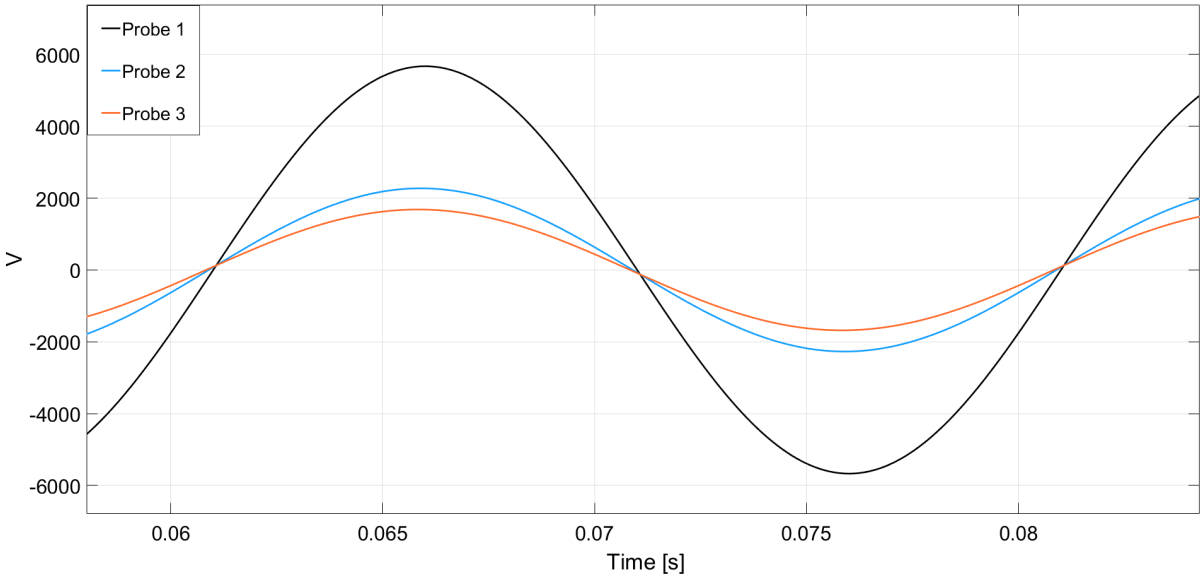

Figure 4.4: Test I: Voltage versus time, circuit without voltage drop in sheath.

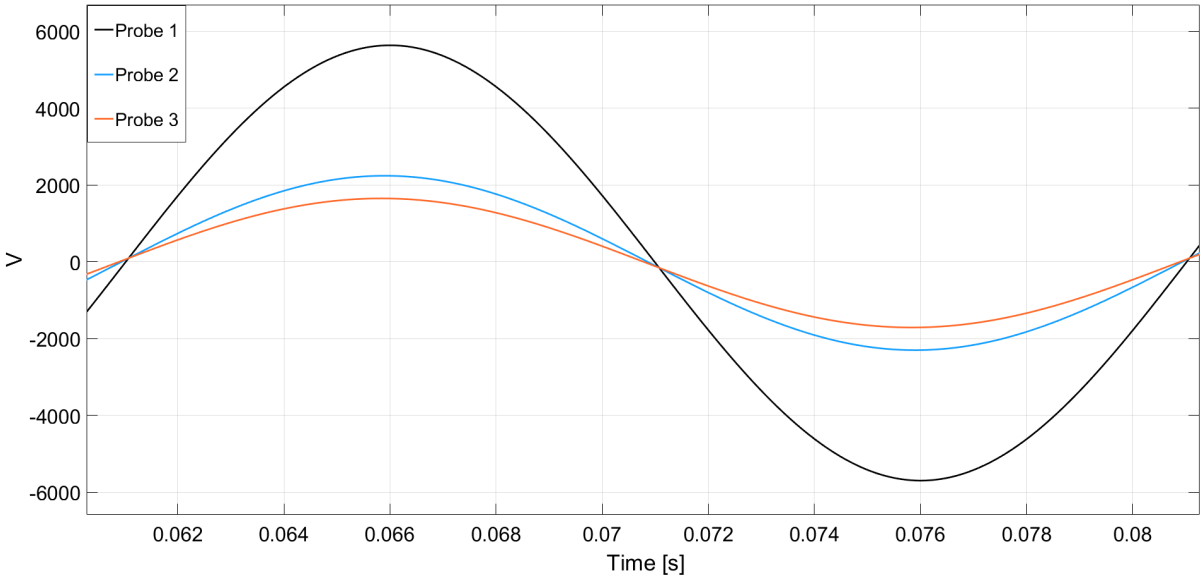

Figure 4.5: Test I: Voltage versus time, circuit with voltage drop in sheath.

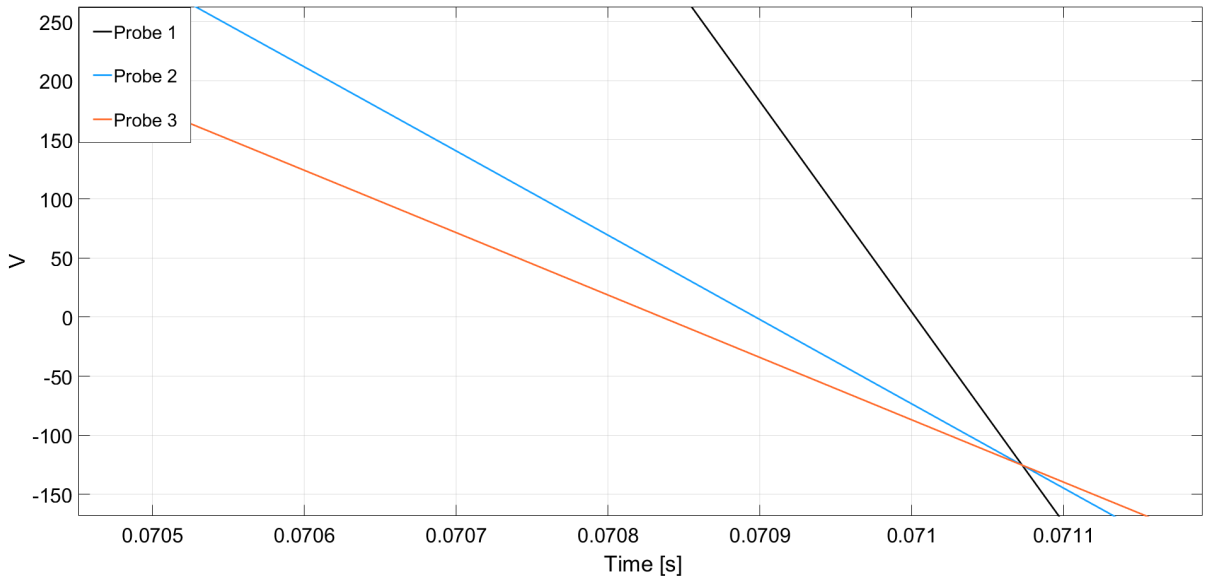

Figure 4.6: Test I: Voltages at zero crossing, circuit without voltage drop in sheath.

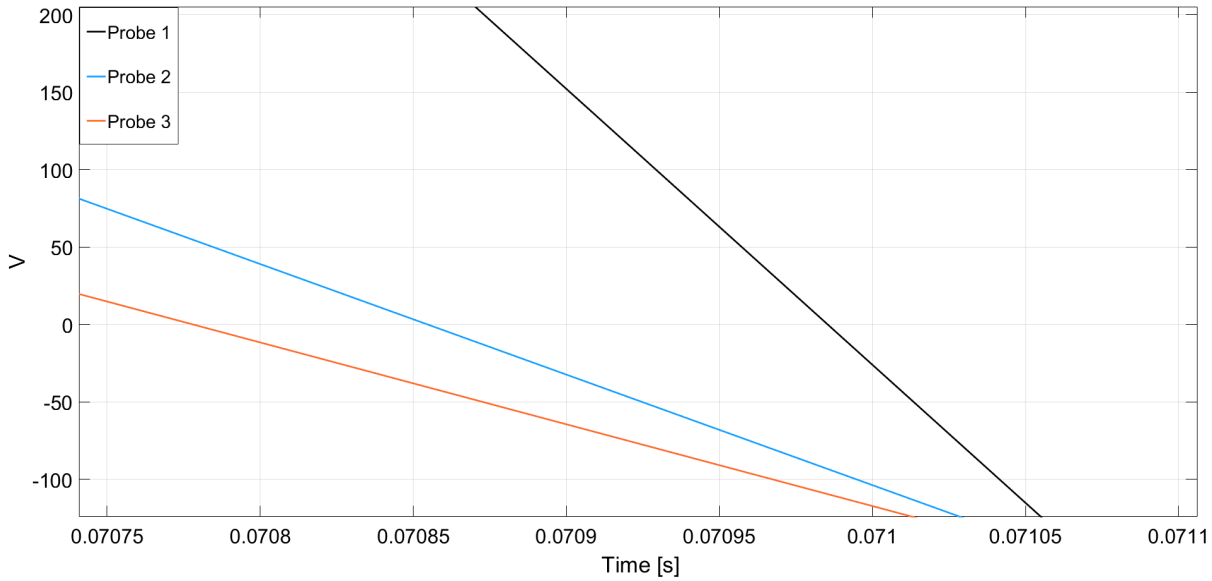

Figure 4.7: Test I: Voltages at zero crossing, circuit with voltage drop in sheath.

The same simulations were done for "Test II" in the Settendal [3] and gave similar results, and are therefore not shown here. It can be assumed, based on this model, that the voltage drop over the sheath is most likely not the problem. Since this model is very simple, it was also tested if subtracting the calculated voltage drop from the measurement would give reasonable results. The resulting change was small at best, and ended up being negligible. All in all, it was not found anything that could allow the sheath's effect to become large enough to serve as the sole reason for this shift.

4.3 Frequency Response Measurement

Another factor was also considered as being able to generate these shifts, notably the frequency response of the probes used. In the measuring circuit, each measuring probe has a large resistance (100 MΩ). The large resistance could result in a poor frequency response. Since the probes consists of RC components, the frequency can be expressed as:

$$f = \frac{1}{2\pi RC} \tag{4.4}$$

Where f is the cutoff frequency, R is the resistance and C is the stray capacitance. With a high resistance, the frequency will thus be very low [2, 11].

To see if the error present in the earlier measurements were caused by the probes, a frequency response measurement was conducted. This was performed by measuring the variation of voltage from the probe tip to the end of the probe. This allows one to see how the circuit elements in the probe influence the measured values. A plot of the result is shown in Fig. 4.8. The measurements start at 50 Hz and goes to 30 MHz.

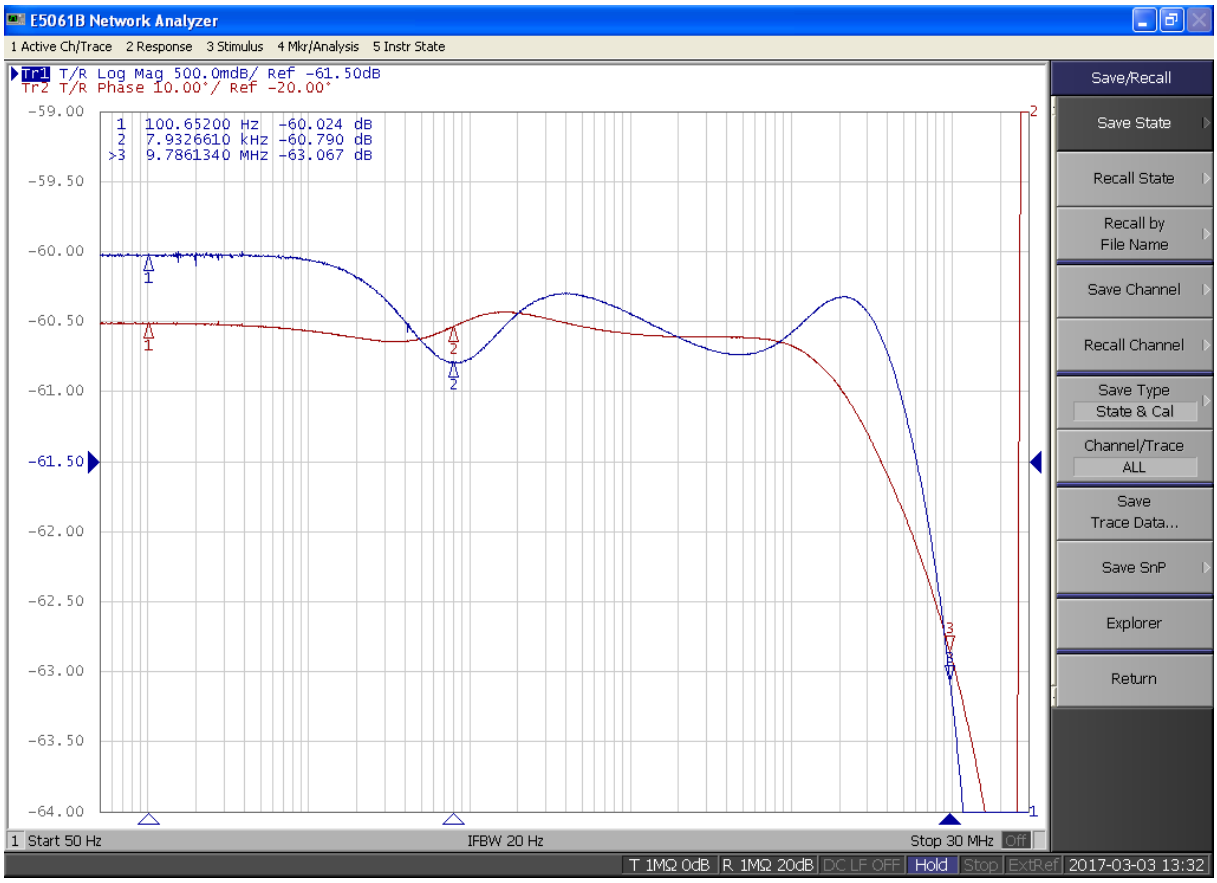

Figure 4.8: Frequency response measurement for one resistive probe.

From the graphs, it can be noted that the curves do not vary notably except when approaching the very high frequency range and the maximum difference is about 3 dB. The conclusion is thus that this is not the reason for the voltage shifts.

4.4 Correction of Measurements

In Settendal [3], the probes had approximately a 90-degree shift in relation to the total voltage, which indicates that there must be some large stray capacitances in the system. Ideally these capacitances should be found for all the measurements. This could be done by measuring the capacitances at the lab. This was not done in this thesis, instead some calculated corrections were added to the measurements. The current drawn by one probe right before and after current zero, can be describes as:

$$i_0 = C\frac{dv}{dt} \tag{4.5}$$

Where i_0 is the drawn current at $t = 0$, C is the stray capacitance, $\frac{dv}{dt}$ is the change in voltage at time t. Ohm's law states that:

$$v = R \cdot i_0 \tag{4.6}$$

Where v is the voltage at time t and R is the resistance. By inserting (4.6) in (4.5), one gets:

$$v_{calculated} = RC\frac{dv}{dt} \tag{4.7}$$

This calculated voltage is then subtracted from the measured voltage, giving a corrected voltage:

$$v_{corrected} = v_{measured} - v_{calculated} \tag{4.8}$$

This correction gave satisfactory results and is therefore applied to all the measurements presented in this work.

Chapter 5

Experimental Results and Discussion

In this chapter, the experimental results are presented. Two different electrode sizes were used, 4.0 mm and 6.0 mm. All the tests were done twice and performed with and without the probes connected. The tests were also conducted with an increased pressure inside the ablation tube, this is referred to as the "self-blast" setup. All ablation tubes were made from the same material.

5.1 Repeatability

The first step that was done at the lab was to validate the experiments repeatability. All the tests were conducted twice with the same setup to check if the repeatability was within acceptable limits. To illustrate this process two of the test are shown below, Fig. 5.1 and Fig. 5.2. From the graphs, it can be seen, that any differences they may have are negligible. This trend was also present in all the other tests, concluding that the experimental setup produces repeatable results.

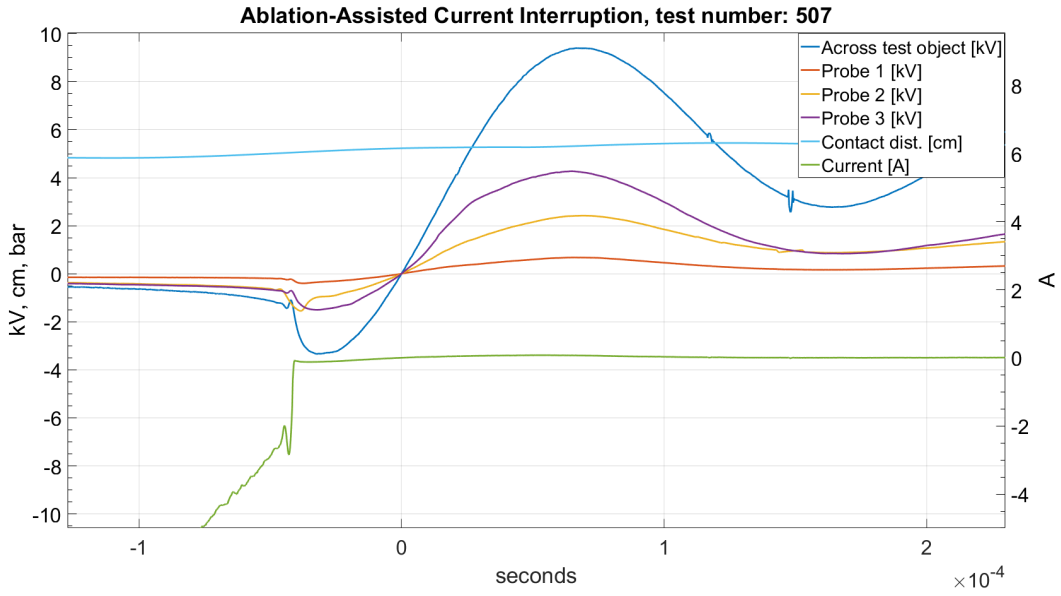

Figure 5.1: Test with 4.0 mm electrode.

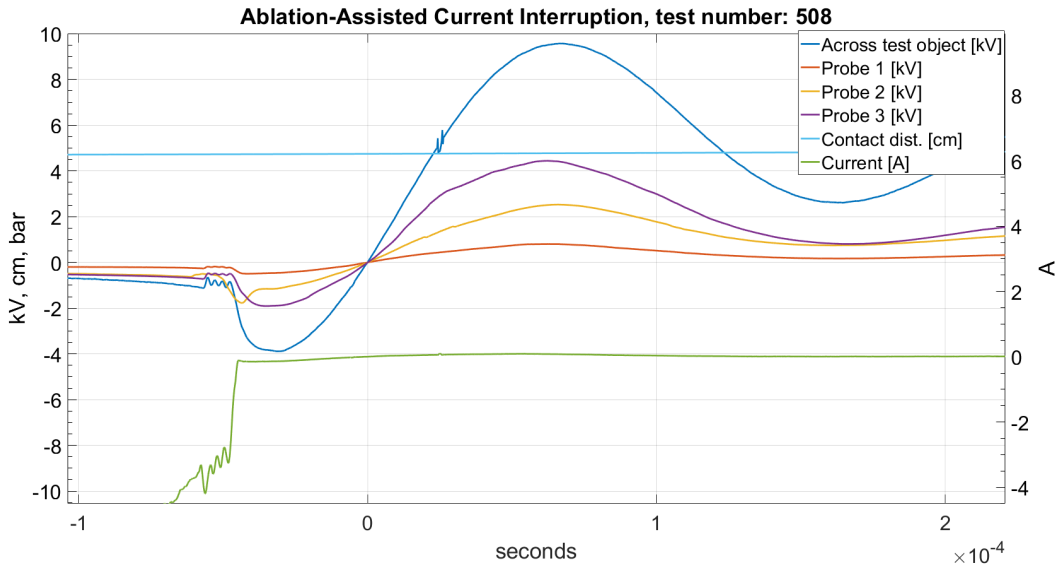

Figure 5.2: Test with 4.0 mm electrode.

5.2 Probe Voltages at Current Zero Crossing

From the voltage measurements that were conducted in this project, it was seen that the probes did not measure 0 V at CZ. The measured voltages are shown in Fig. 5.3, the negative measurements are shown as positive values since the size of the voltage is most important. As seen, the values are considerably larger than zero. Especially the probe right before the gas vent (Probe 2) differs significantly from zero in some of the tests. In test number 518 it measured 1.16 kV. It might be the case that this probe has a higher measuring error, or something in its vicinity influences its measurement capability.

As seen from the figure, tests number 515, 517, 518 and 519 have very high values for Probe 2. All these four tests were done with the 6.0 mm electrode. In tests 518 and 519 the "self-blast" setup is used. Although Probe 2 has the largest offsets, Probe 3 seems to have the highest overall error. All the measured voltages are listed in Appendix B, Table B.1.

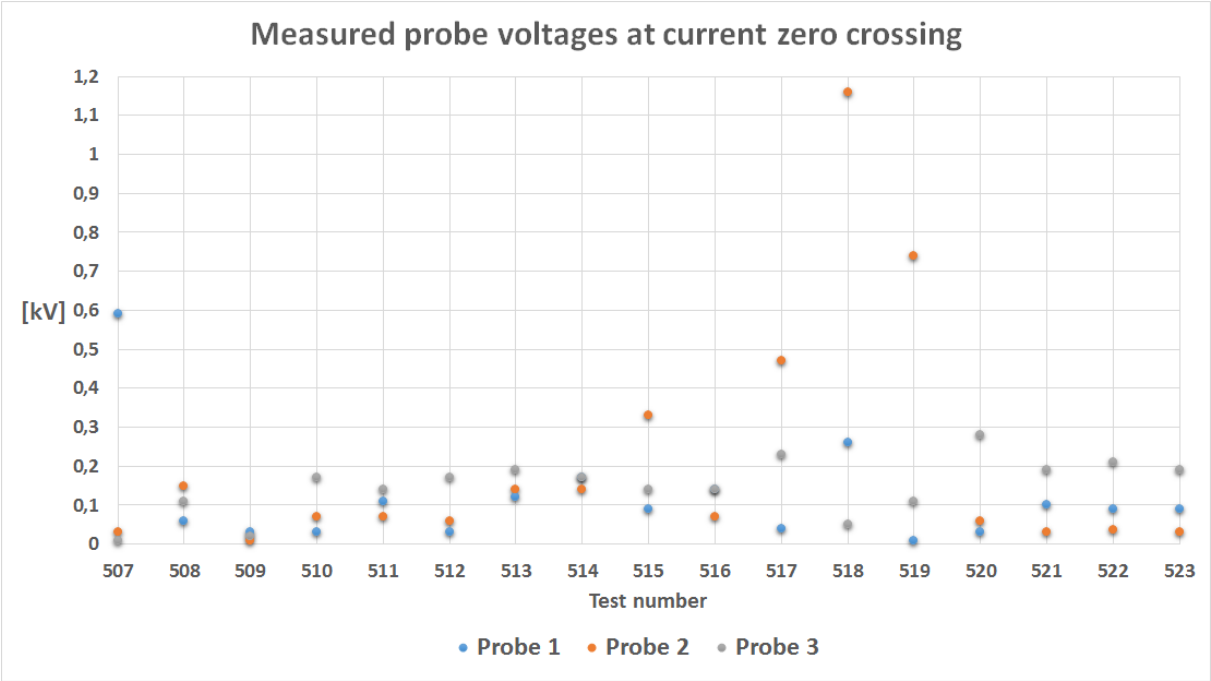

Figure 5.3: Scatter plot showing how much voltage the probes measure at CZ.

5.3 Impact of Voltage Shift Correction

To view the impact the correction method has on the measurement data, two plots are shown to compare the corrected and uncorrected values. Fig. 5.4 is a test with the 4.0 mm electrode with no "self-blast". As seen, the probe voltages reach zero at different times. In Fig. 5.5 the values are corrected and they now cross zero at the same instant.

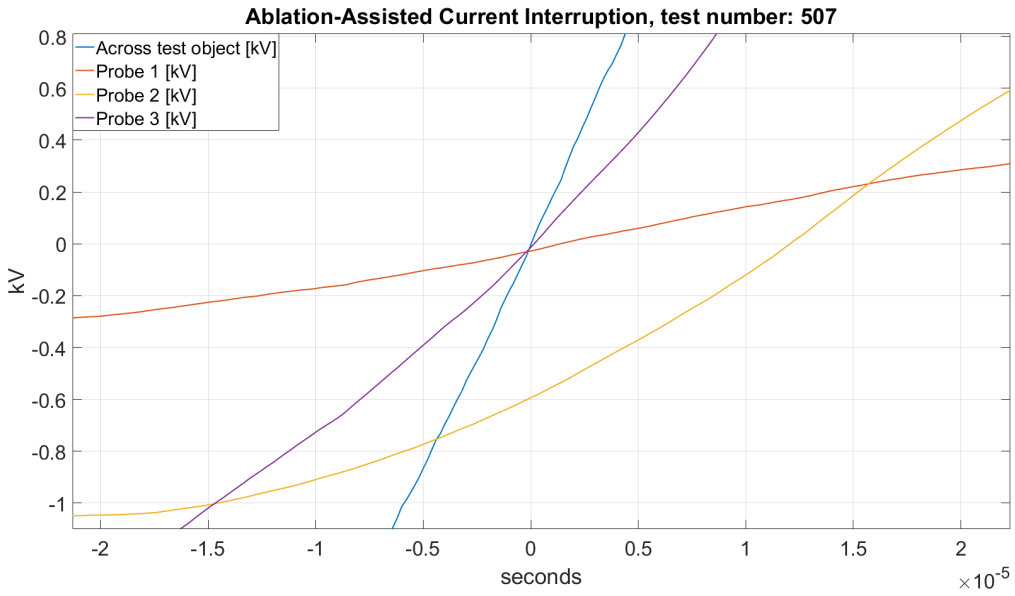

Figure 5.4: 4.0 mm electrode. No correction applied to curves.

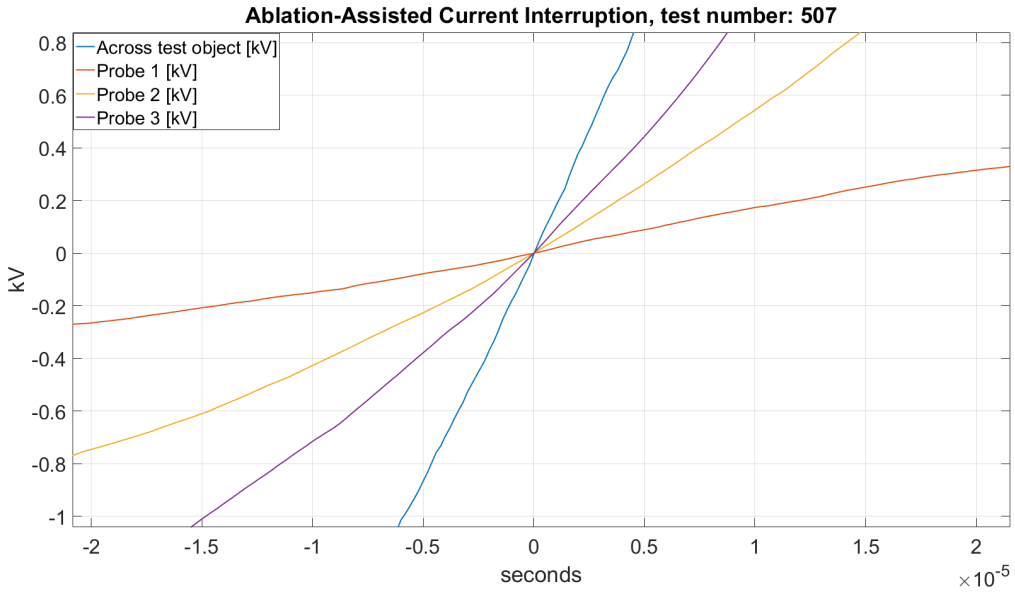

Figure 5.5: 4.0 mm electrode. With correction applied to curves.

5.4 The Time Interval that Results are Considered Valid

The electrical circuit for one probe is shown in Fig. 5.6, the probe is not perfectly isolated from the test object and will therefore draw some current. The total amount of current drawn by the probes, will dictate whether the measurements can be considered valid. In the post-arc region, the total current through the plasma arc is very small. The total current drawn by the probes is therefore no longer small compared to that through the switch. This will affect the system in such a way that the probe currents can no longer be neglected.

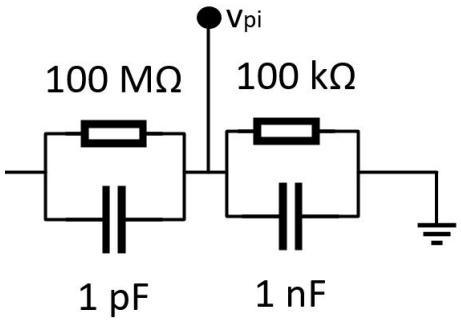

Figure 5.6: Electrical circuit for one probe, it consists of a high voltage part and a low voltage part.

To determine the time interval where the measurements are valid, the sum of the currents drawn by the probes and the total current running through the switch must then be compared.

If it is assumed that all the probe current runs through the low voltage portion of the probe, an expression for the current drawn by a single probe can be written as:

$$i_{p_i} = C\frac{dv_{p_i}}{dt} + \frac{v_{p_i}}{R} \tag{5.1}$$

Where i_{p_i} is the current running through probe i, C and R are the components of the low voltage part, $C\frac{dv_{p_i}}{dt}$ is the capacitive current and $\frac{v_{p_i}}{R}$ is the resistive current. The voltage gradient over the probe is calculated by using two different points on the voltage curve. The measurements are assumed to be valid if:

$$i_{total} >> \sum i_{p_i} \tag{5.2}$$

Where i_{total} is the total current running through the plasma arc and $\sum i_{p_i}$ is the sum of the calculated probe currents. The assumption is that if i_{total} is much larger than the sum of the probe currents, the voltage measurements are considered valid.

The calculated probe currents and the total current through the switch at different times, are shown in Fig. 5.7 and 5.8, for one test with "self-blast" and one without. From the graphs, it is seen that the measurements are valid for at least 100 μs after current interruption. After 100 μs, the difference between the currents is too small to be considered valid. They are also considered valid for all measurements before CZ crossing, since the current through the switch is much higher than the sum of currents, flowing through the probes. The blue curves in the figures are multiplied with a factor, to make it visible. Thus, the difference is even larger than it appears in the figures.

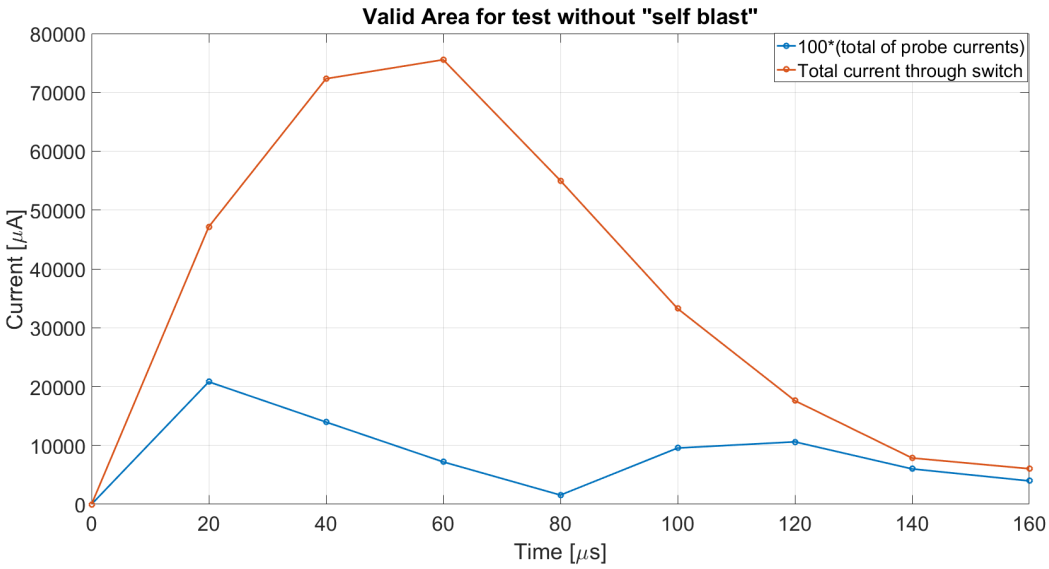

Figure 5.7: Test 507: Total current through the switch and sum of calculated probe currents.

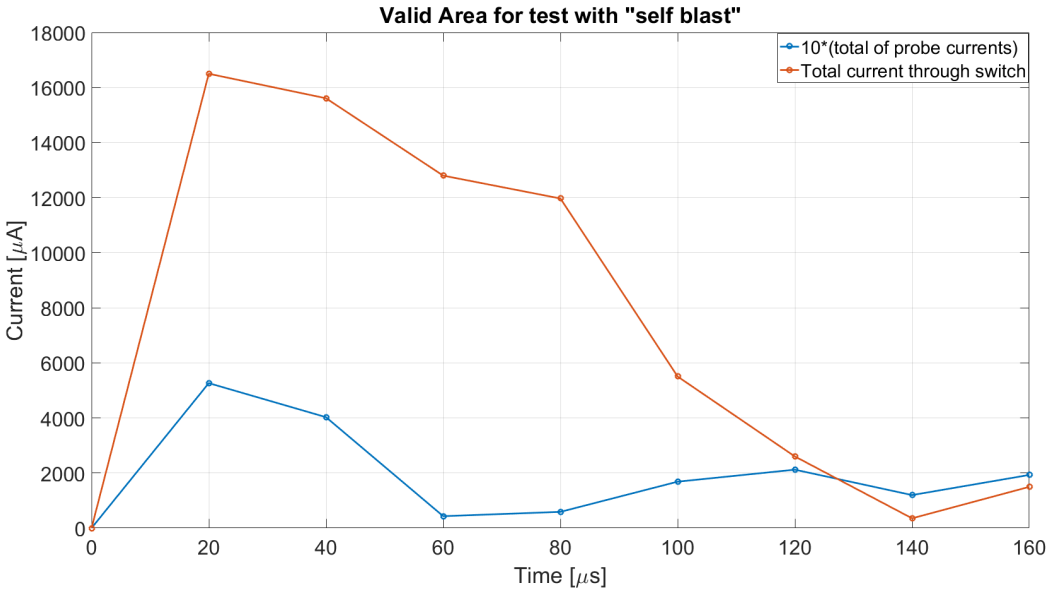

Figure 5.8: Test 505: Total current through the switch and sum of calculated probe currents.

5.5 Reviewing the Effect by the Probes on the Measured Voltage over the Test Object

The tests were conducted with and without the screws and tungsten wire, to see what impact these had on the measurements. The screws were made of nylon, and there will be some sharp edges from the drilling of the holes which could have an impact on the measurements.

5.5.1 Tests With 4.0 mm Electrode, No "Self-Blast"

To show whether the probes have a significant impact on the measurements, two tests are plotted together, as shown in Fig. 5.9 and Fig. 5.10. In test number 507 the probes are connected, and in test 510 they are not. The probe voltages are not plotted since the measurement across the whole test object will show the difference between the setups.

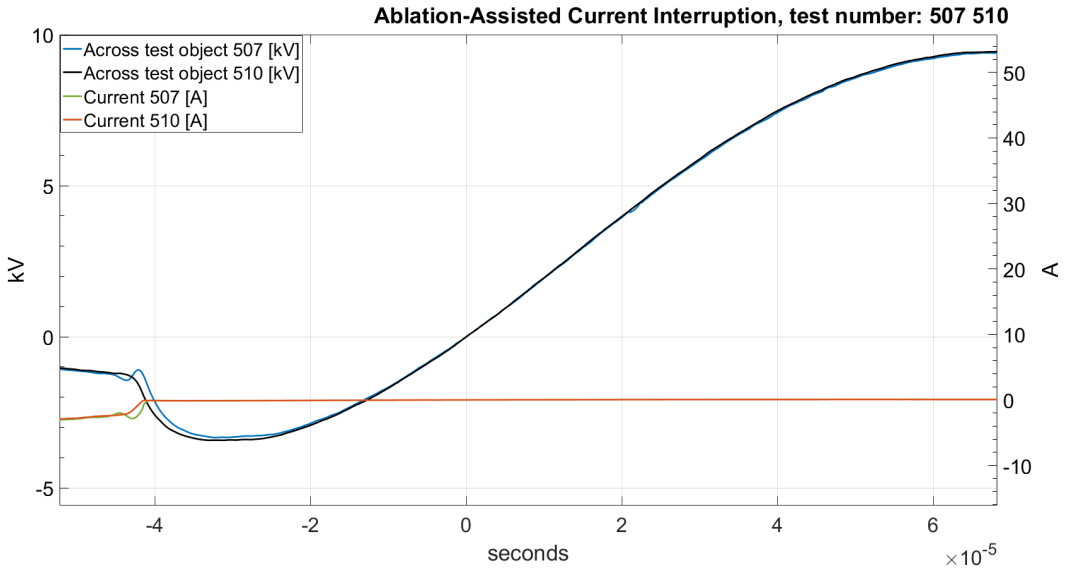

Figure 5.9: Test 507 is with probes and test 510 is without.

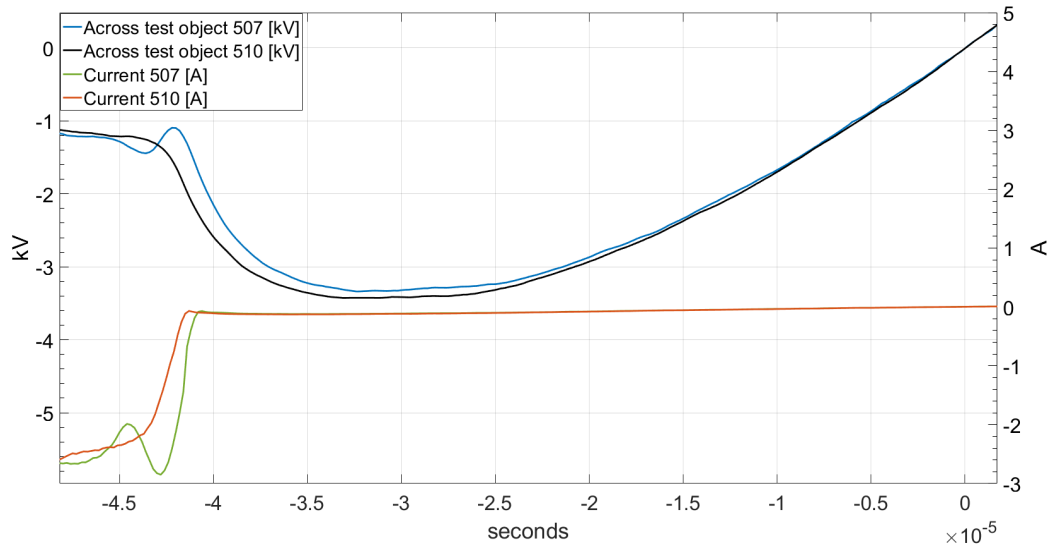

Figure 5.10: Test 507 is with probes and test 510 is without. Zoomed in view.

As seen, the curves follow each other closely, the largest difference is at about 40 μs before CZ.

5.5.2 Tests With 4.0 mm Electrode, With "Self-Blast"

Tests were also conducted where the switch was made to act like a "self-blast" circuit breaker. This was done by closing the left side of the switch by mounting the device market as number 7 in Fig. 3.2. Test number 506 was conducted with the probes connected, and in test 513 they were not. The two tests are plotted together in Fig. 5.11 and 5.12.

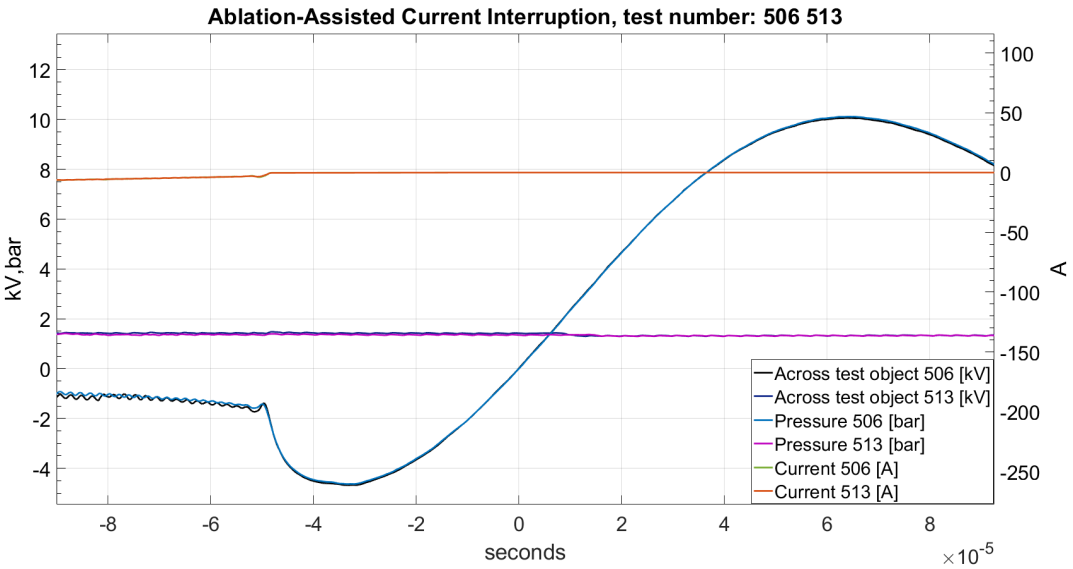

Figure 5.11: Test 506 is with probes connected and 513 is without. The "self-blast" setup is used.

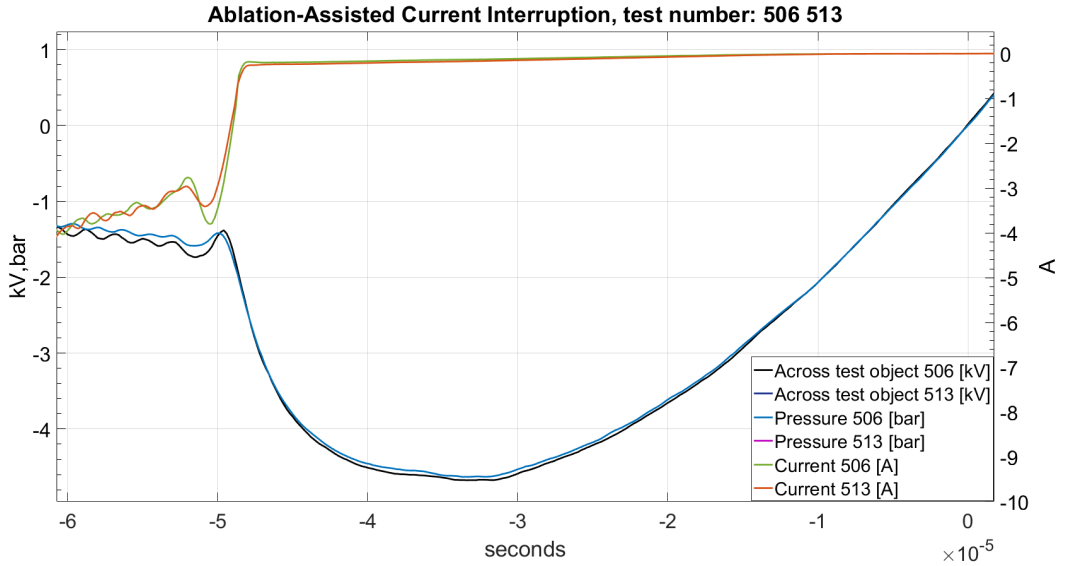

Figure 5.12: Test 506 is with probes connected and 513 is without. The "self-blast" setup is used. Zoomed in view.

As seen from the figures, the probes do not have any significant impact on the voltage. The

curves follow each other closely and the pressure is 1.4 bar for both tests.

5.5.3 Tests With 6.0 mm Electrode, No "Self-Blast"

The measured voltages over the whole test object, using the 6.0 mm electrode, are shown in Fig. 5.13 and 5.14. Test number 515 has the probes connected and test 522 is without. Again, the curves almost follow the same path.

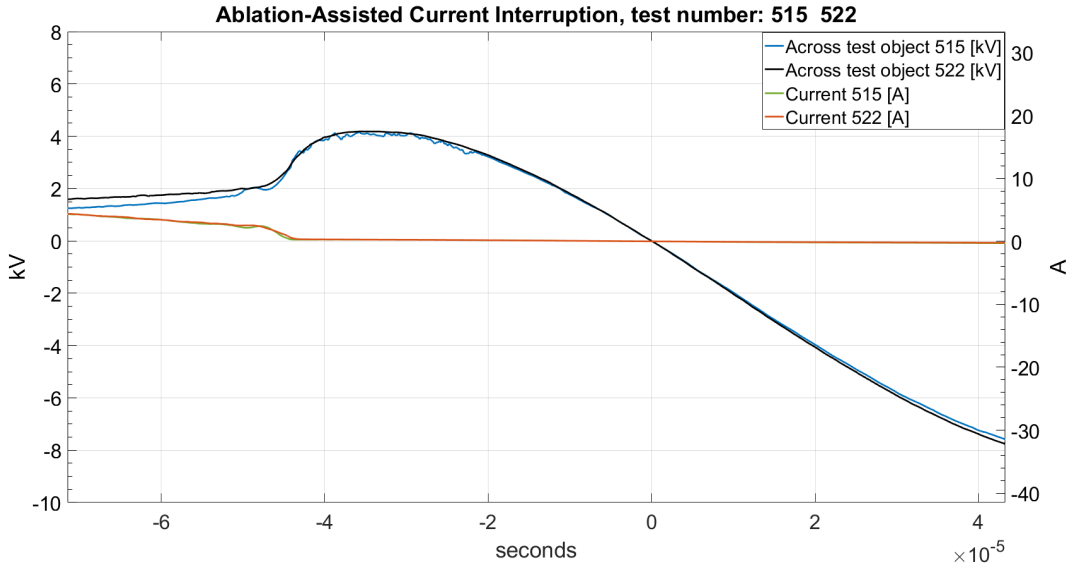

Figure 5.13: Test 515 is with probes connected.

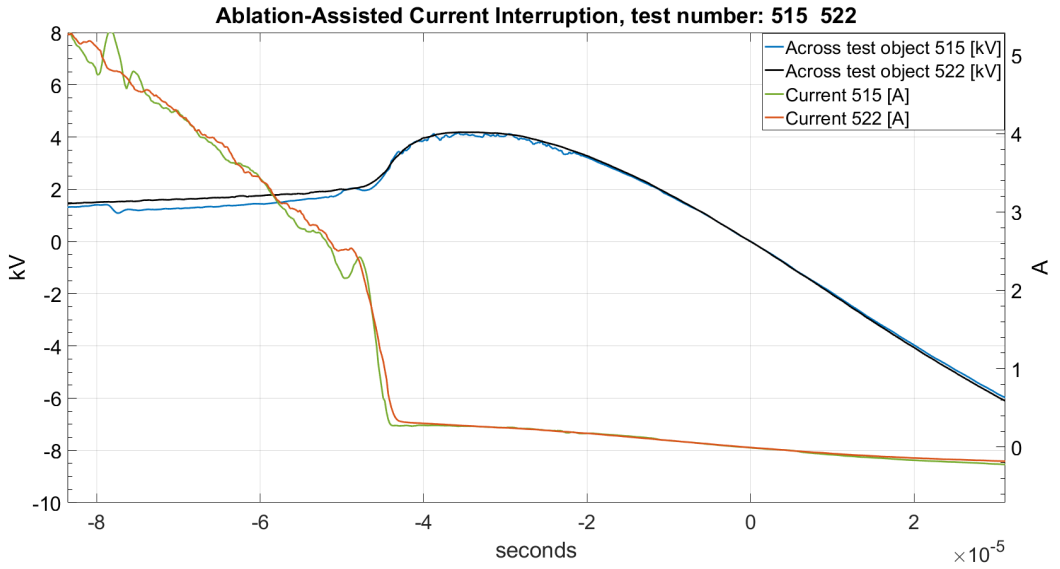

Figure 5.14: Test 515 is with probes connected. Zoomed in view.

5.5.4 Tests With 6.0 mm Electrode, With "Self-Blast"

As seen from Fig. 5.15 and 5.16, introducing the "self-blast" gives higher difference between the curves right before CZ. The pressures are very different, 3.1 bar for the test without probes and 0.7 bar for the other. The current is interrupted at approximately 6.4 and 6.9 cm, for test number 519 and 520 respectively. The high pressure in test number 519 is most likely due to the smaller volume between the electrode and attachment point. A decrease in volume gives an increase in pressure.

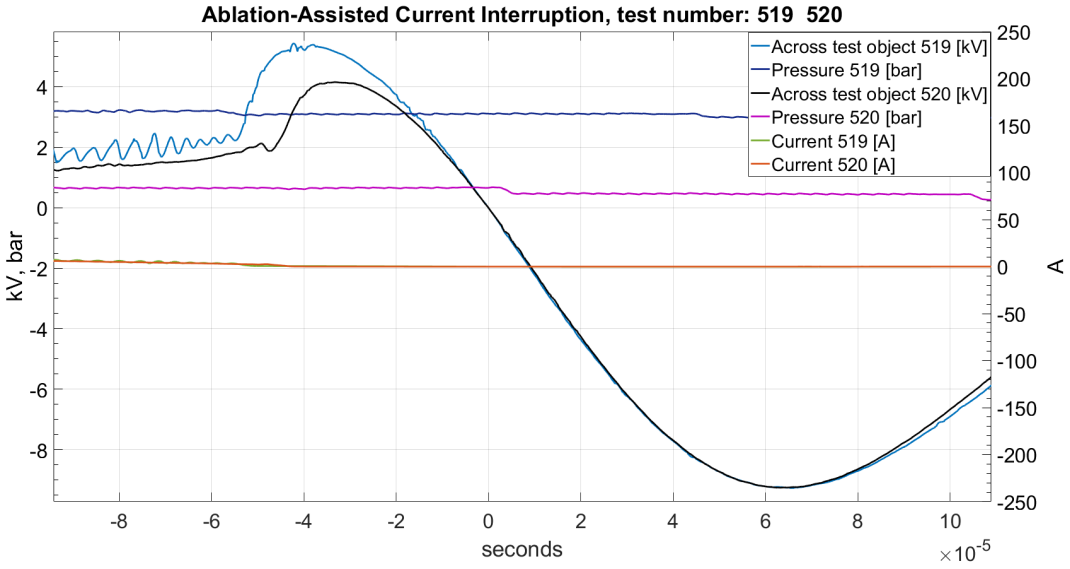

Figure 5.15: Test 519 is with probes connected. The "self-blast" setup is used.

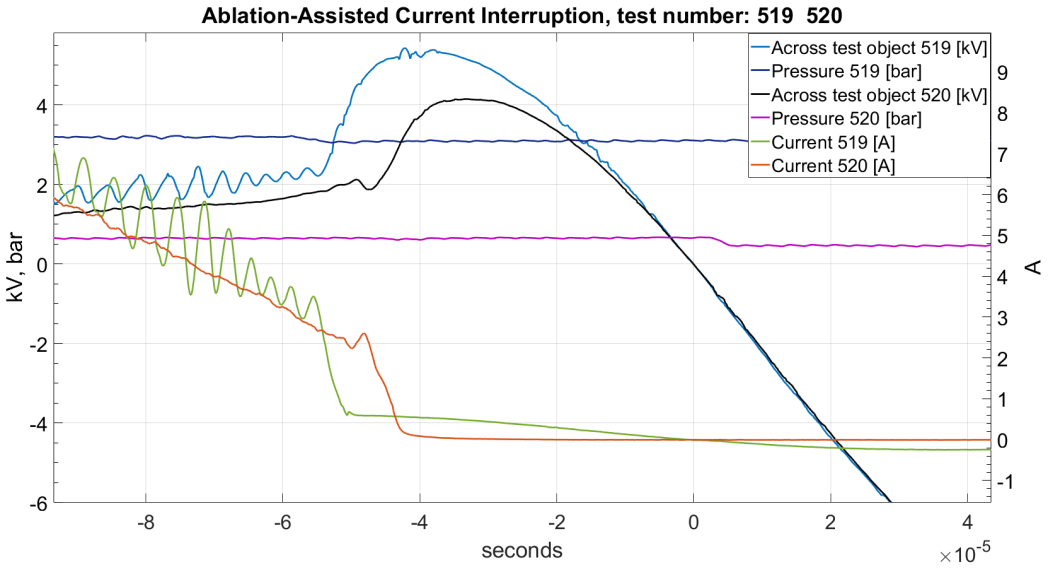

Figure 5.16: Test 519 is with probes connected. The "self-blast" setup is used. Zoomed in view.

5.6 Arc Voltage Extinction Peak for Tests With and Without the "Self-Blast" Setup

Along with the arc conductance, the arc voltage peak that occurs a few moments before current zero can give good indications on the interrupting capability of a breaker. This peak in voltage is called the arc voltage extinction peak [12]. A higher peak indicates that more energy is being removed from the arc prior to its extinction, thus giving an easier interruption [13].

5.6.1 Tests With 4.0 mm Electrode

In Fig. 5.17 the arc voltage extinction peaks for two tests with the 4.0 mm electrode are plotted. Test number 505 is done with the "self-blast" setup and test 507 is without.

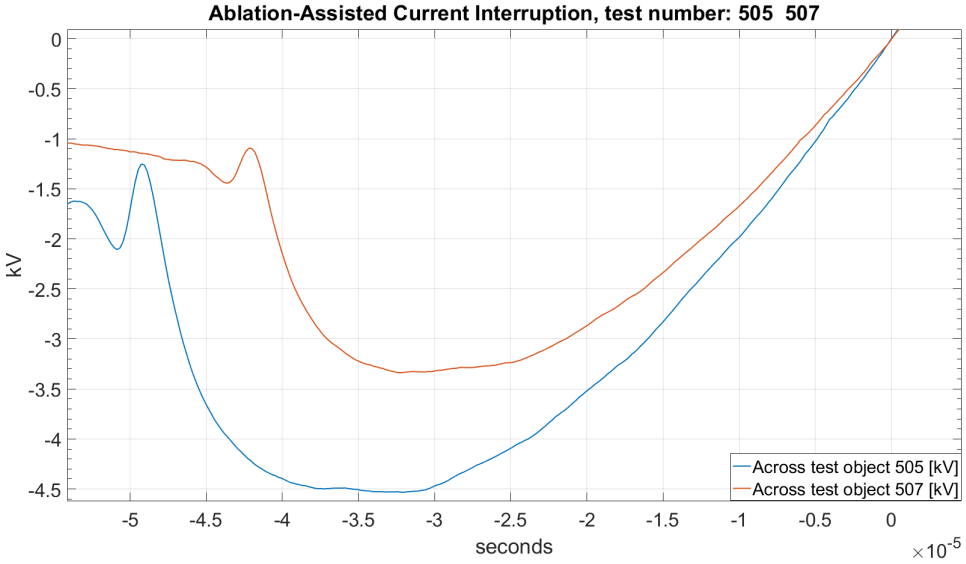

Figure 5.17: The voltage peaks right before CZ crossing.
Test 505 is with "self-blast".
Test 507 is without "self-blast".

As seen from the figure, the voltage peak for the test with "self-blast" is larger. It is about 1.2 kV higher, which gives better breaking capability.

5.6.2 Tests With 6.0 mm Electrode

The same comparison as in the previous chapter was done for the 6.0 mm electrode. The curves are shown in Fig. 5.18, where test 518 is the one with "self-blast". Again, utilizing the arc energy to interrupt the current gives a higher arc voltage extinction peak. The increase is now about 1.1 kV, which is just 100 volts less than it was for the 4.0 mm electrode.

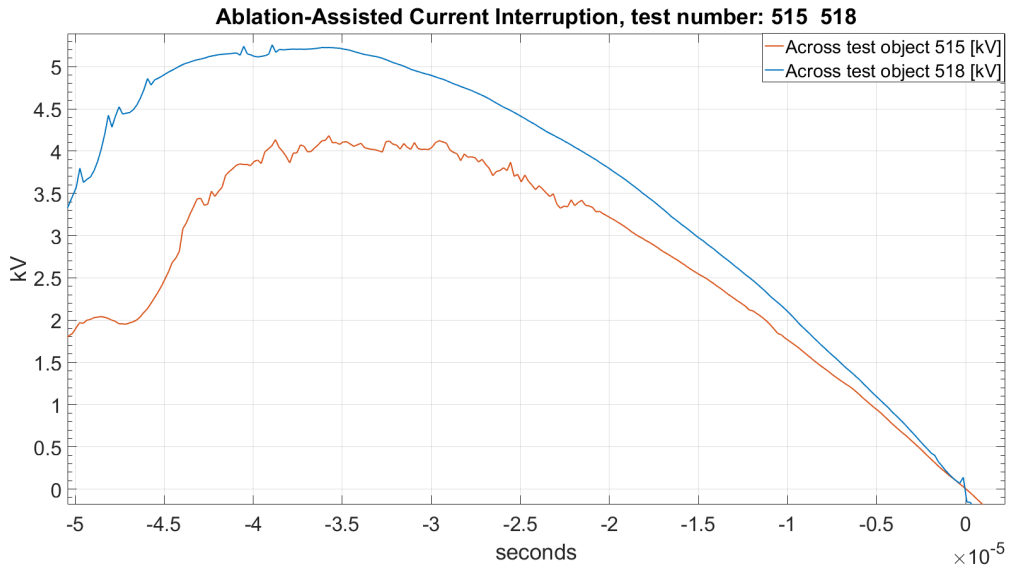

Figure 5.18: The voltage peaks right before CZ crossing.
Test 518 is with "self-blast".
Test 515 is without "self-blast".

5.7 Breaking Current for Tests With and Without the "Self-Blast" Setup

An increase in arc extinction voltage will in general also mean that the breaking current increases [13]. The breaking current is the current right before a successful current interruption. Higher current creates more ablation, thus improving the breaking capability [7]. Comparisons of tests with and without the "self-blast" setup are done for both electrode dimensions.

5.7.1 Tests With 4.0 mm Electrode

Fig. 5.19 shows the breaking currents, where test number 505 is the one with the "self-blast" setup. As predicted, the breaking current for test 505 had a larger peak. One can also see that the curve oscillates more and peaks earlier. The difference in peak values is about 1.4 A.

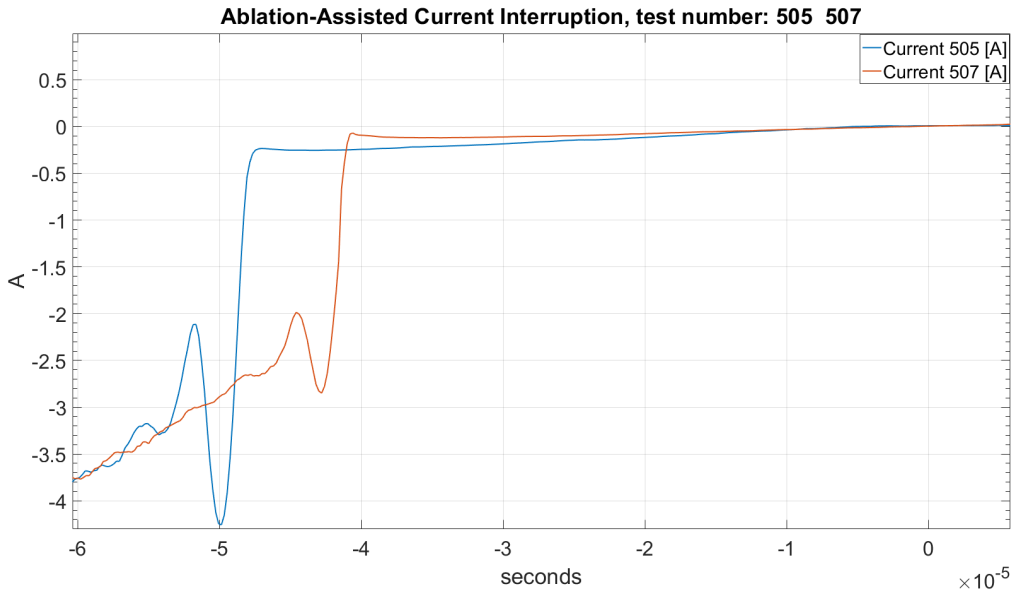

Figure 5.19: The currents right before CZ crossing.
Test 505 is with "self-blast".
Test 507 is without "self-blast".

5.7.2 Tests With 6.0 mm Electrode

As seen in Fig. 5.20, the setup with the "self-blast", again has a higher breaking current peak. The difference in peaks is now about 0.7 A, which is half of what it was with the 4.0 mm electrode.

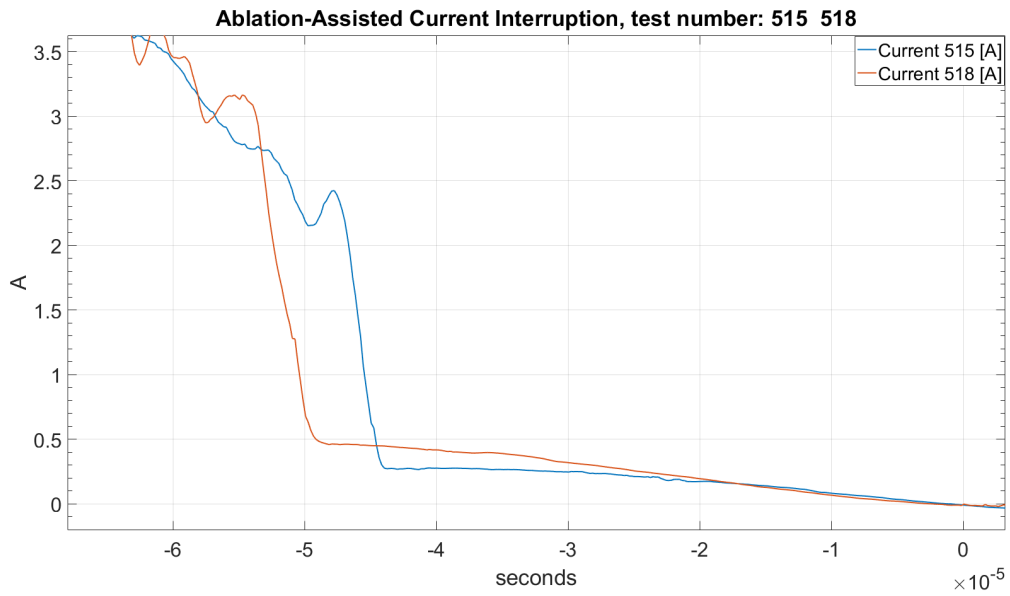

Figure 5.20: The currents right before CZ crossing.
Test 518 is with "self-blast".
Test 515 is Without "self-blast".

5.8 Post-arc Currents for Tests With and Without the "Self-Blast" Setup

Large post-arc currents increase the chance for thermal run-aways and therefore increases the risk of re-ignitions. It also wears down the breaker much quicker [7]. The post-arc currents in the interval 1.2 μs after CZ crossing, are shown in Fig. 5.21. The plot shows the tests with the 4.0 mm electrode. As seen, the "self-blast" effect reduces the post-arc current.

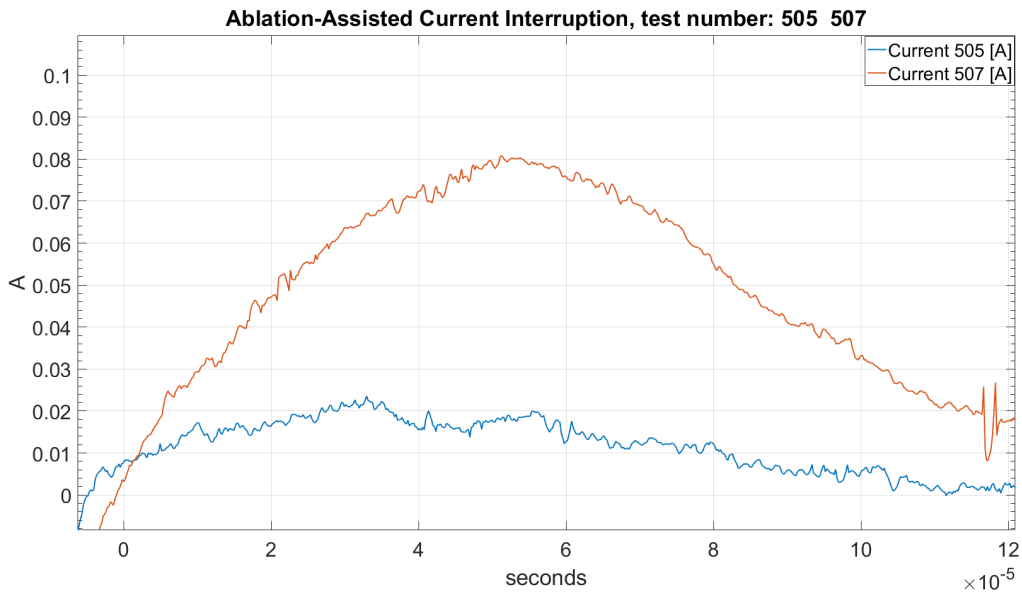

Figure 5.21: The currents right after CZ crossing.
Test 505 is with "self-blast".
Test 507 is without "self-blast".

The post-arc currents when using the 6.0 mm electrode are shown in Fig. 5.22. The post-arc current is again lower when using the "self-blast" setup.

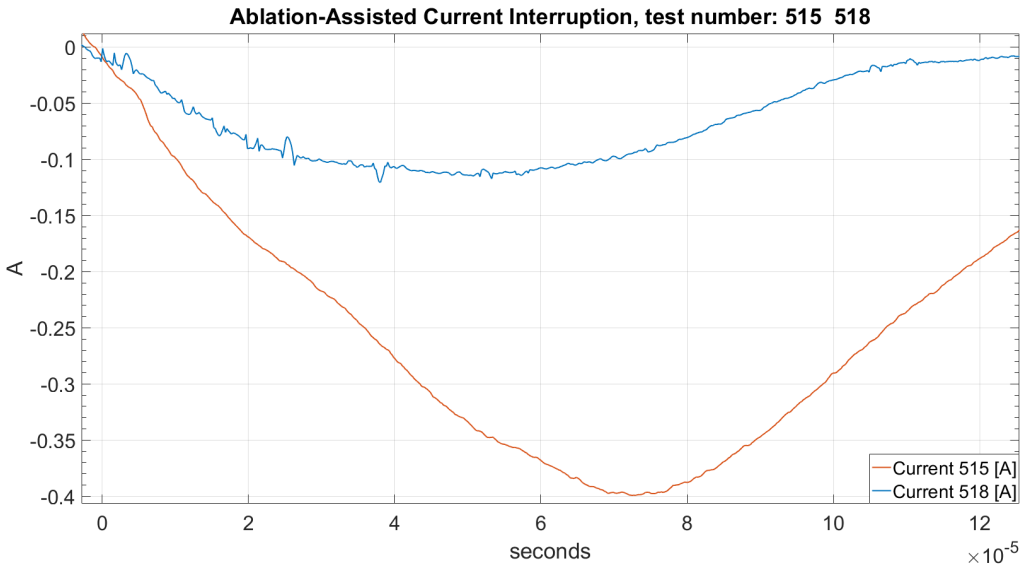

Figure 5.22: The currents right after CZ crossing.
Test 518 is with "self-blast".
Test 515 is without "self-blast".

5.9 Distribution of the Arc Voltage

It is interesting to look at how the arc voltage is distributed, before and after the CZ crossing. In the following sections the voltage distributions are plotted for the different setups. All the values are taken at 20 μs, before and after the CZ crossing.

In the tables "section 1...3" refers to the distances between the probes, as shown in Fig. 3.4a. The three first sections are in total 24.8 mm. Section 4 is calculated by taking the distance the electrode has traveled and subtract 24.8 mm from this value.

5.9.1 Tests With 4.0 mm Electrode. Setup Without "Self-Blast"

The voltages and current are shown in Fig. 5.23, for some μs before and after current zero crossing.

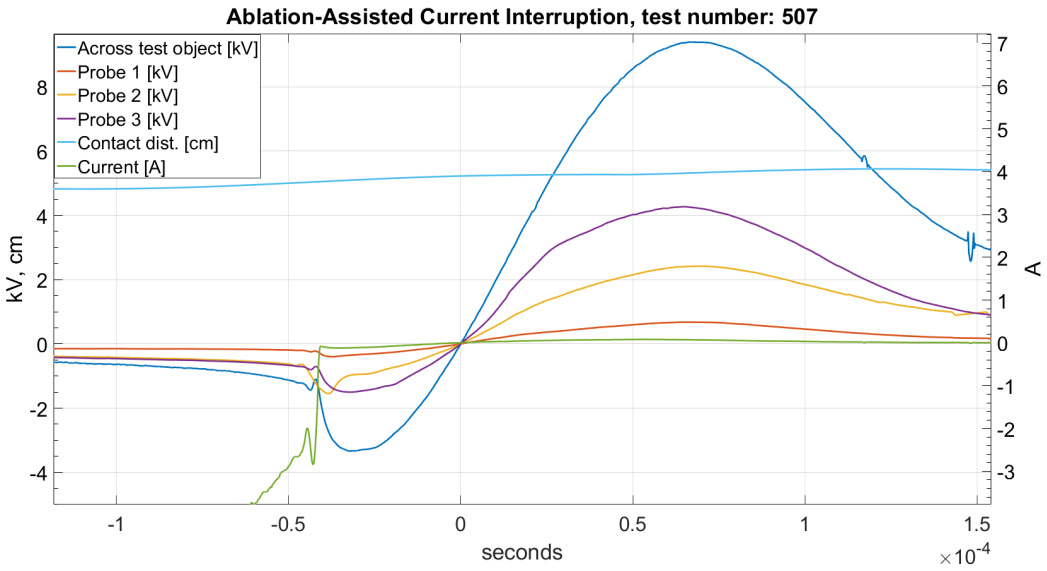

Figure 5.23: Measured voltages and current, for test with 4.0 mm electrode and no "self-blast".

Before CZ crossing

A plot of the voltages and current right before CZ, is shown in Fig. 5.24. By analyzing the curves at 20 μs before CZ, the calculations for voltage distribution and field strength are as shown in Table 5.1. The electrode has traveled 5 cm and the current is 77 mA.

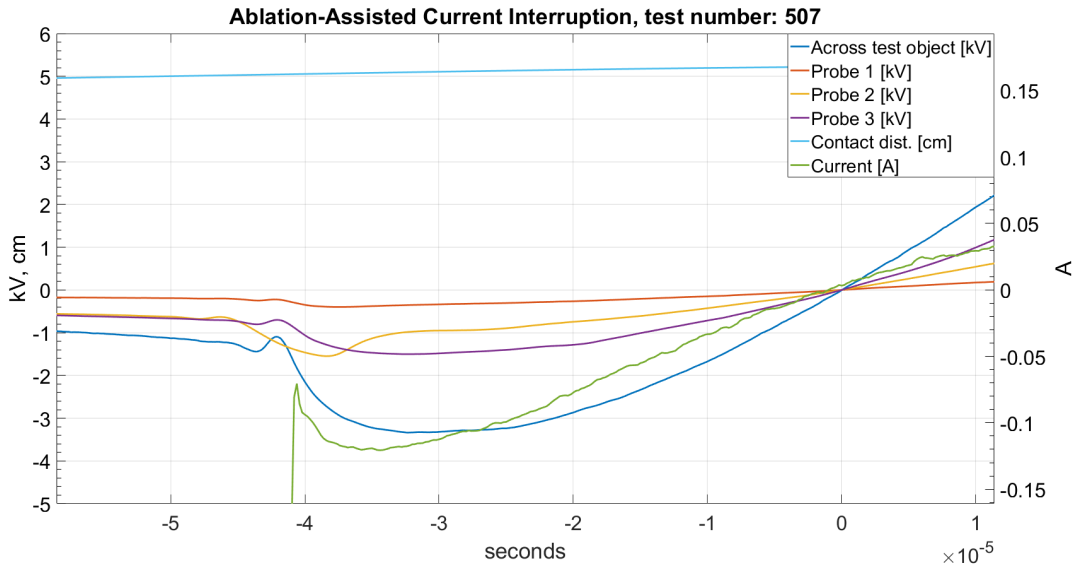

Figure 5.24: Measured voltages before CZ, for test with 4.0 mm electrode and no "self-blast".

Table 5.1: Test 507; Voltage and field strength distribution of the arc.
t = - 20 μs, i = 77 mA.

	Section 1	Section 2	Section 3	Section 4	Total
Length [mm]	6.6	12	6.2	26.7	51.5
Voltage difference [kV]	0.3	0.5	0.5	1.7	3.0
Percentage of total voltage [%]	10	16.7	16.7	56.6	100
Field strength [kV/mm]	0.045	0.042	0.081	0.064	

After CZ crossing

In Fig. 5.25 the measured voltages right after current zero are shown. By extracting the voltage values right after CZ crossing and calculating the difference between the them, the voltage differences and field strengths are found to be as shown in Table 5.2. The current is 47 mA at 20 μs and the electrode has traveled a bit further than 5 cm.

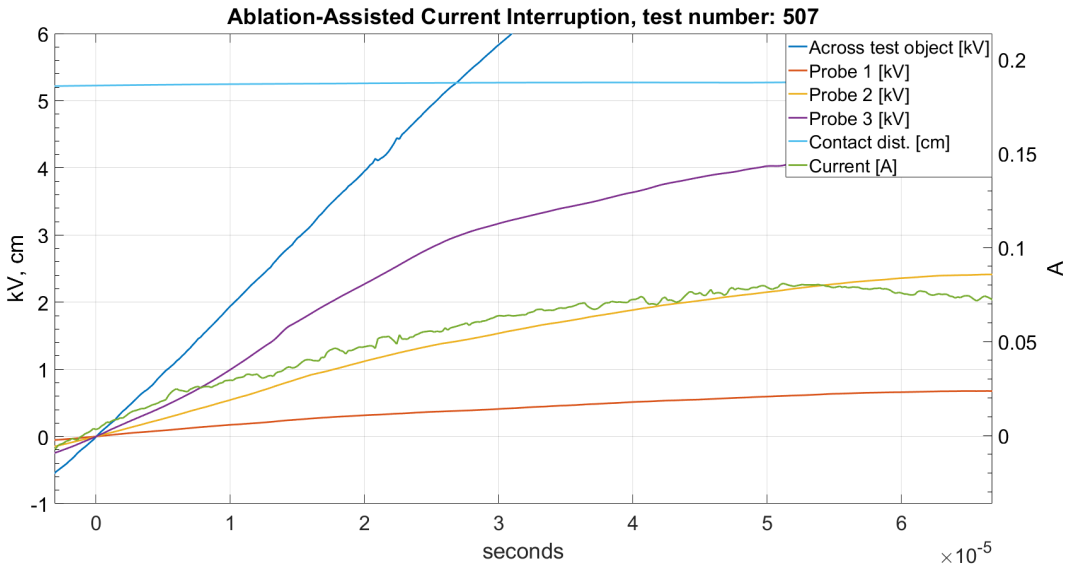

Figure 5.25: Post-arc voltages for test with 4.0 mm electrode and no "self-blast".

Table 5.2: Test 507; Voltage and field strength distribution of the arc.
$t = 20\ \mu s$, $i = 47$ mA.

	Section 1	Section 2	Section 3	Section 4	Total
Length [mm]	6.6	12	6.2	27.9	52.7
Voltage difference [kV]	0.3	0.8	1.2	1.7	4.0
Percentage of total voltage [%]	7.5	20	30	42.5	100
Field strength [kV/mm]	0.045	0.067	0.194	0.061	

As seen from Table 5.2, most of the voltage is distributed over "section 4", which is logical since this section is long compared to the others. It is also clear that much of the voltage is also over "section 3", which is where the gas outlet is located. Since "section 3" is much shorter, the field strength will be significantly higher, as shown in the table.

5.9.2 Tests With 6.0 mm Electrode. Setup Without "Self-Blast"

The measured voltages and the current through the switch, are plotted in Fig. 5.26.

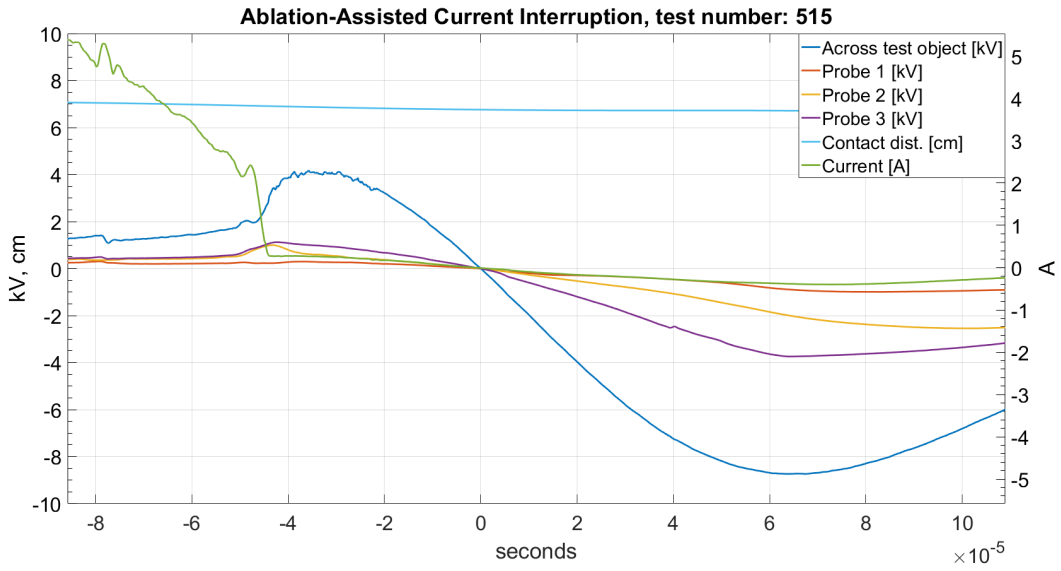

Figure 5.26: Measured voltages and current, for test with 6.0 mm electrode and no "self-blast".

Before CZ crossing

The voltages and current for the test with the 6.0 mm electrode, are plotted for a few micro seconds before CZ in Fig. 5.27. The calculated voltage distribution and field strengths are shown in Table 5.3. The electrode has traveled about 6.8 cm and the current is 174 mA. The field strength is now largest in section 4.

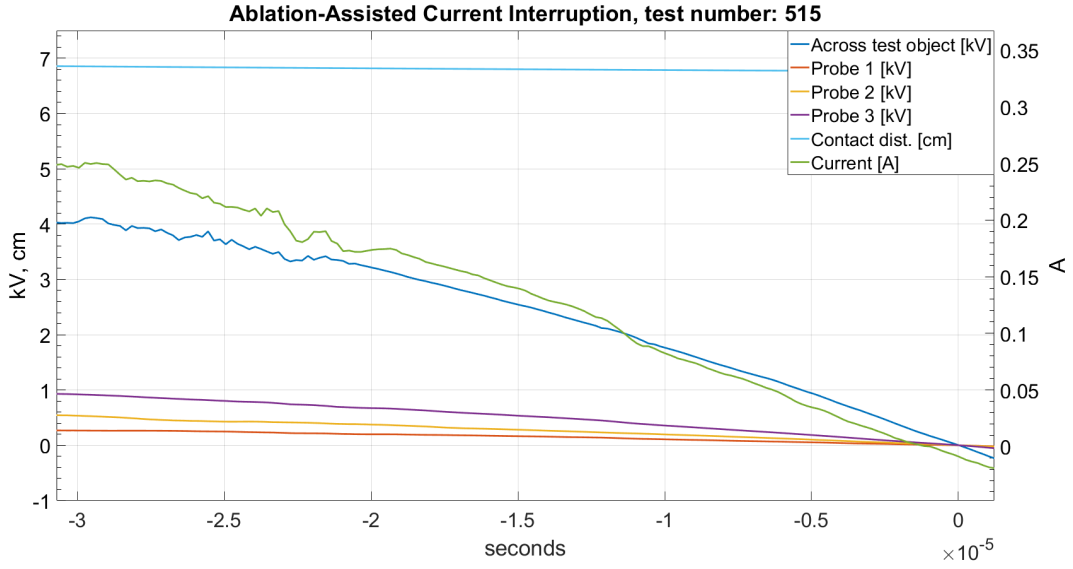

Figure 5.27: Measured voltages before CZ, for test with 6.0 mm electrode and no "self-blast".

Table 5.3: Test 515; Voltage and field strength distribution of the arc.
t =-20 μs, i = 174 mA.

	Section 1	Section 2	Section 3	Section 4	Total
Length [mm]	6.6	12	6.2	43.4	68.2
Voltage difference [kV]	0.2	0.2	0.3	2.5	3.2
Percentage of total voltage [%]	6.25	6.25	9.4	78.1	100
Field strength [kV/mm]	0.030	0.017	0.048	0.058	

After CZ crossing

In Fig. 5.28 the post-arc voltages are shown. The electrode has traveled 6.7 cm and the current is 169 mA. The findings are presented in Table 5.4. As seen, the field strength is now largest in section 3.

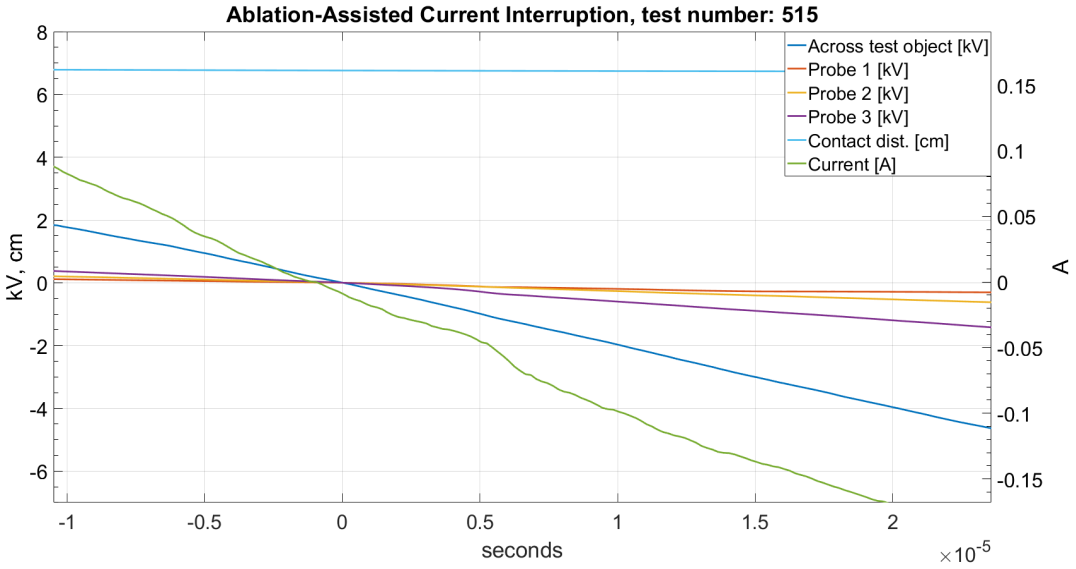

Figure 5.28: Post-arc voltages for test with 6.0 mm electrode and no "self-blast".

Table 5.4: Test 515; Voltage and field strength distribution of the arc.
t = 20 μs, i = 169 mA.

	Section 1	Section 2	Section 3	Section 4	Total
Length [mm]	6.6	12	6.2	42.6	67.4
Voltage difference [kV]	0.3	0.2	0.7	2.8	4.0
Percentage of total voltage [%]	7.5	5	17.5	70	100
Field strength [kV/mm]	0.045	0.017	0.113	0.066	

5.9.3 Tests With 4.0 mm Electrode. Setup With "Self-Blast"

For this setup, the measurements are shown in Fig. 5.29. As seen, the probes cannot measure above ca. 5 kV, this is because all the probes are grounded to the same point which limits their range.

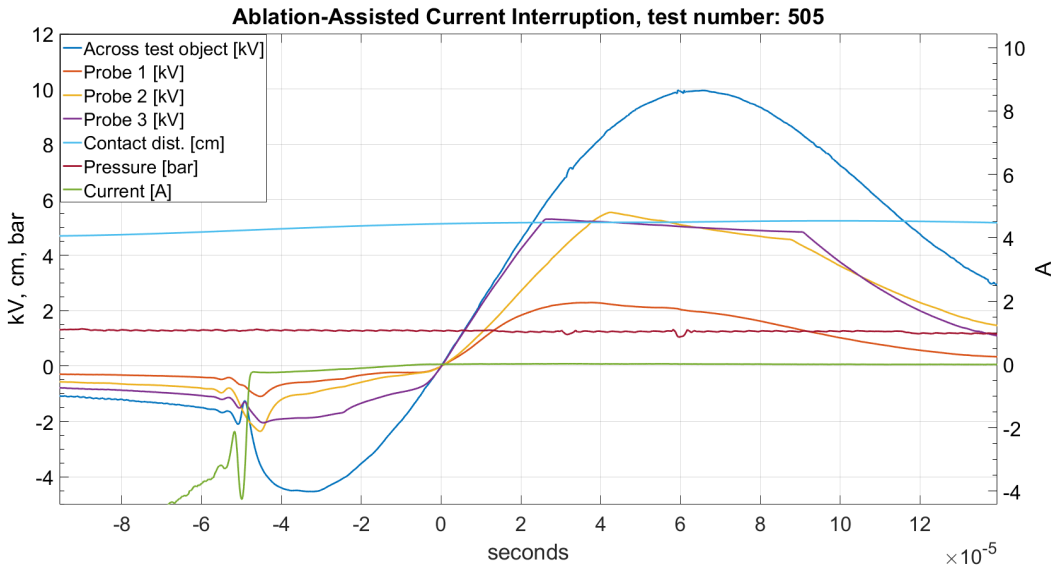

Figure 5.29: Measured voltages and current, for test with 4.0 mm electrode and with "self-blast".

Before CZ crossing

The voltages and current are shown in Fig. 5.30, for the test with the 4.0 mm electrode. The calculations are shown in Table 5.5. The electrode has traveled 5 cm and the current is here 117 mA.

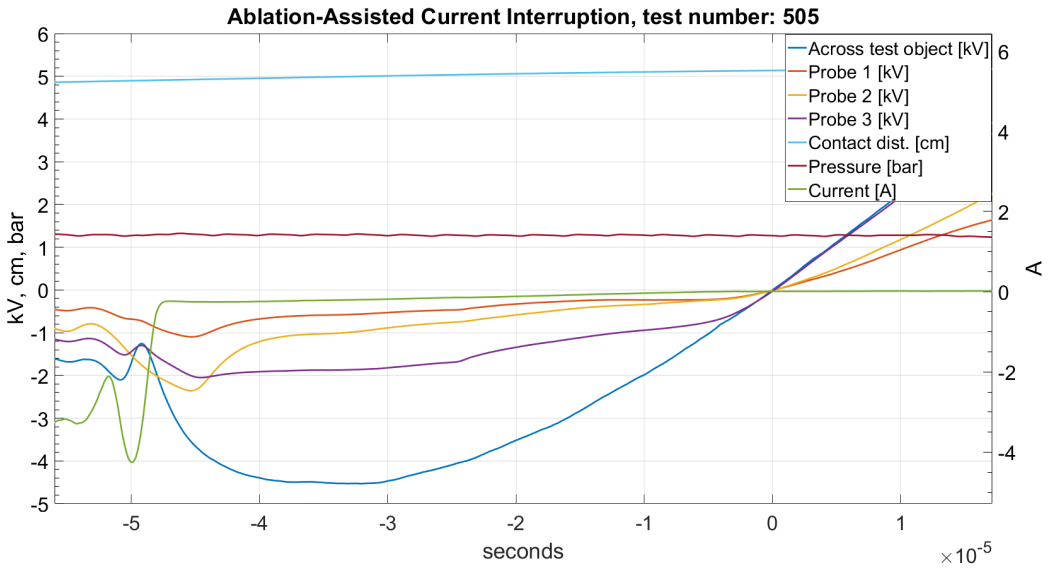

Figure 5.30: Measured voltages before CZ, for test with 4.0 mm electrode and with "self-blast".

Table 5.5: Test 505; Voltage and field strength distribution of the arc.
t =-20 μs, i = 117 mA, p = 1.3 bar.

	Section 1	Section 2	Section 3	Section 4	Total
Length [mm]	6.6	12	6.2	25.8	50.6
Voltage difference [kV]	0.3	0.3	0.7	2.2	3.5
Percentage of total voltage [%]	8.6	8.6	20	62.8	100
Field strength [kV/mm]	0.045	0.025	0.113	0.085	

After CZ crossing

The voltages and current after CZ, are shown in Fig. 5.31. The pressure is 0.9 bar and the current is 17 mA, at 20 μs.

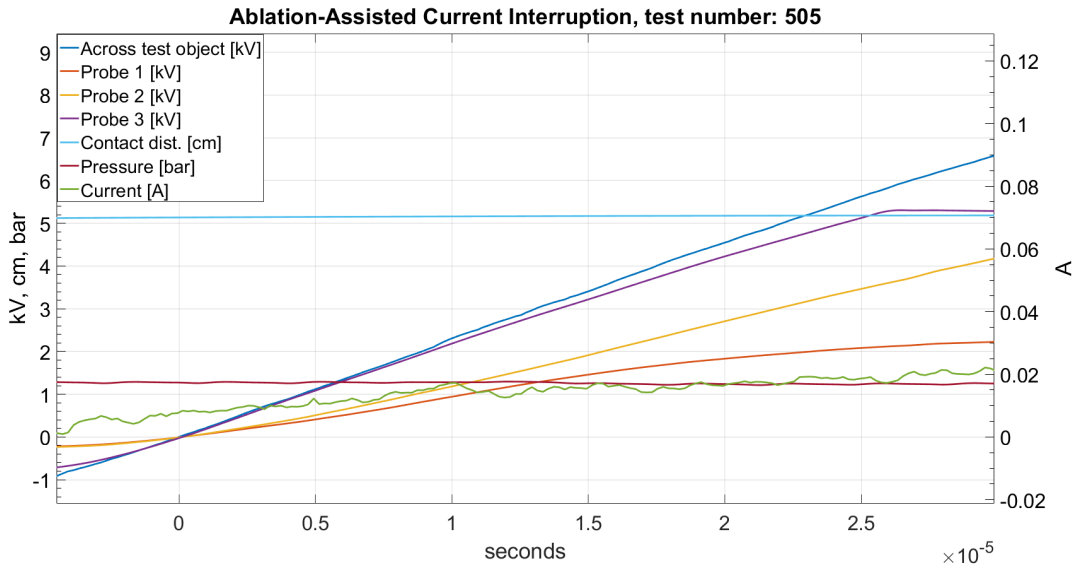

Figure 5.31: Post arc voltages for test with 4.0 mm electrode and "self-blast".

The distribution is shown in Table 5.6. As seen, the field strength in the first section has increased significantly, compared to before CZ. Almost the entire voltage is distributed over the three first sections.

Table 5.6: Test 505; Voltage and field strength distribution of the arc.
t = 20 μs, i = 17 mA, p = 1.2 bar.

	Section 1	Section 2	Section 3	Section 4	Total
Length [mm]	6.6	12	6.2	26.6	51.4
Voltage difference [kV]	1.8	0.9	1.5	0.4	4.6
Percentage of total voltage [%]	39.1	19.6	32.6	8.7	100
Field strength [kV/mm]	0.273	0.075	0.242	0.015	

5.9.4 Tests With 6.0 mm Electrode. Setup With "Self-Blast"

The complete plot for the test with 6.0 mm electrode and "self-blast", is shown in Fig. 5.32.

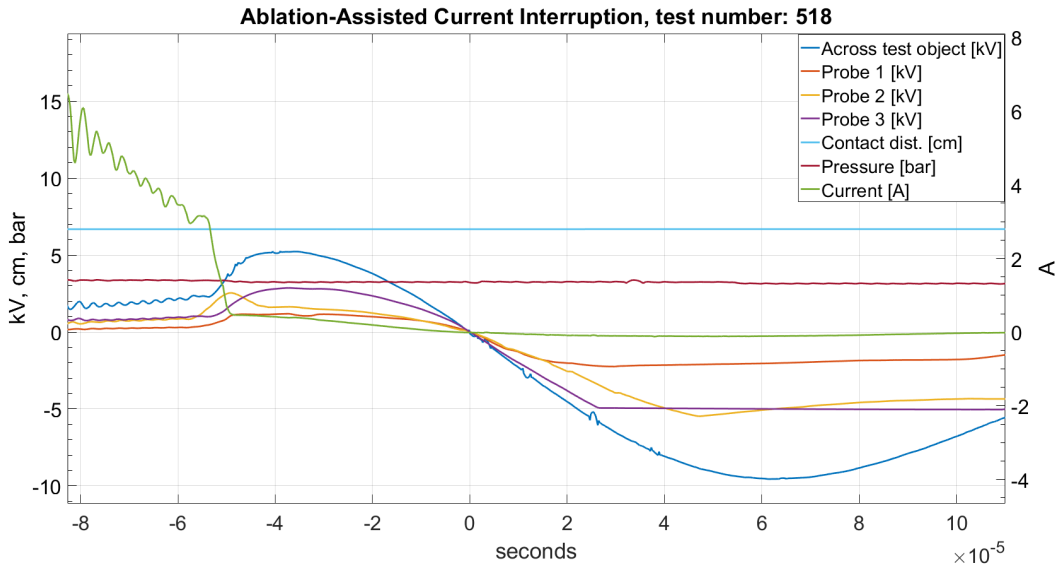

Figure 5.32: Measured voltages and current, for test with 6.0 mm electrode and with "self-blast".

Before CZ crossing

Fig. 5.33 shows the curves a few micro seconds before CZ. The calculations are shown in Table 5.7. As seen, the field strengths in section 1 and 3 are almost the same. The pressure is 3.3 bar, the current is 195 mA and the electrode has traveled 6.7 cm.

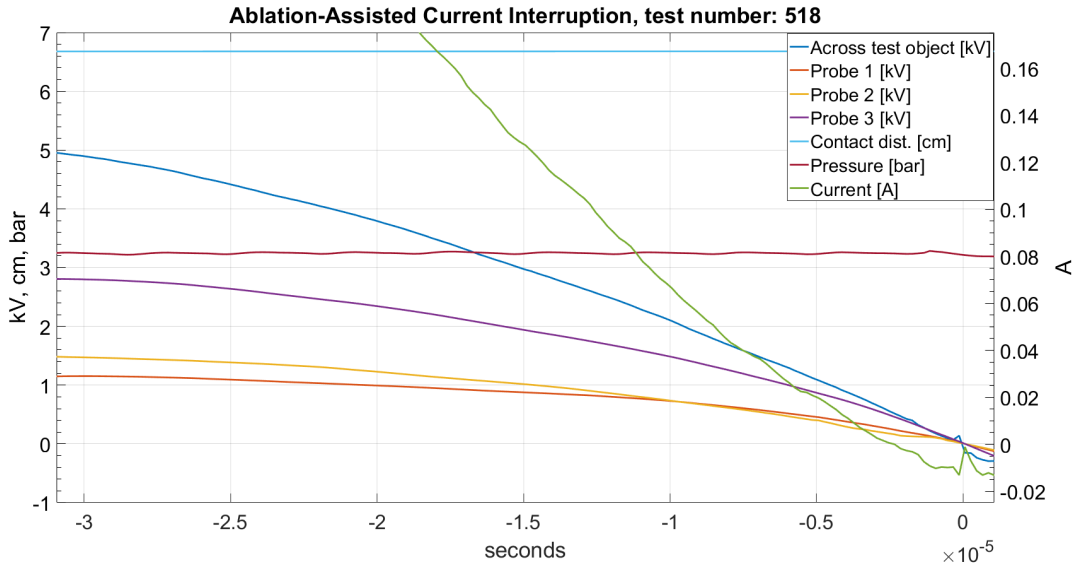

Figure 5.33: Measured voltages before CZ, for test with 6.0 mm electrode and with "self-blast".

Table 5.7: Test 518; Voltage and field strength distribution of the arc.
t =-20 μs, i = 195 mA, p = 3.3 bar.

	Section 1	Section 2	Section 3	Section 4	Total
Length [mm]	6.6	12	6.2	42	66.8
Voltage difference [kV]	1.0	0.2	1.1	1.5	3.8
Percentage of total voltage [%]	26.3	5.3	28.9	39.5	100
Field strength [kV/mm]	0.152	0.042	0.177	0.036	

After CZ crossing

The curves after CZ are shown in Fig. 5.34. The contact distance is still 6.7 cm, the pressure is 8.6 bar and the current is 90 mA. As seen from Table 5.8, the field strength is in this case highest in section 1.

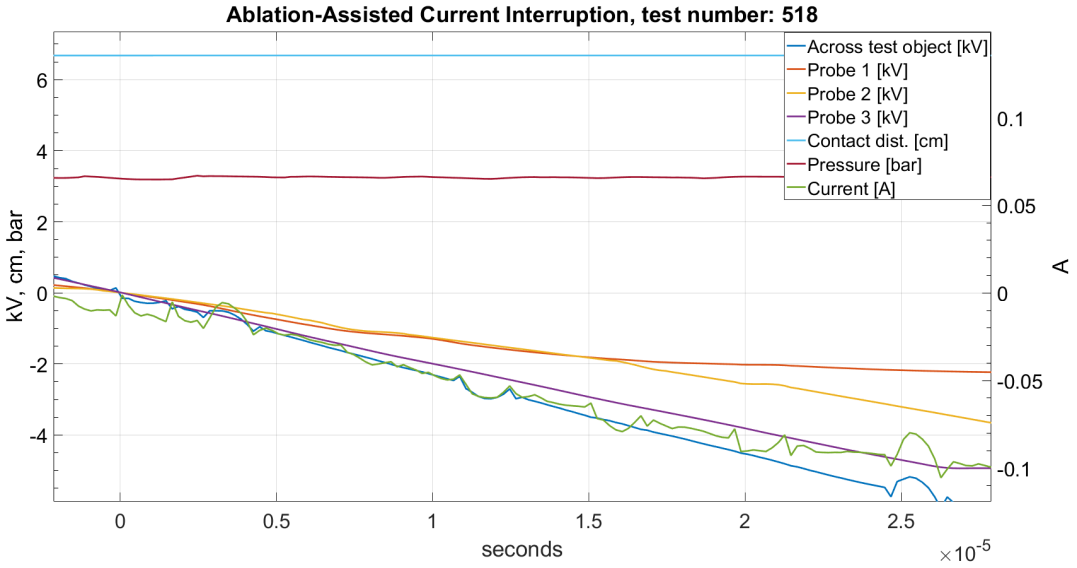

Figure 5.34: Post-arc voltages with 6.0 mm electrode and "self-blast".

Table 5.8: Test 518; Voltage and field strength distribution of the arc.
t = 20 μs, i = 90 mA, p = 3.3 bar

	Section 1	Section 2	Section 3	Section 4	Total
Length [mm]	6.6	12	6.2	42	66.8
Voltage difference [kV]	2.0	0.6	1.2	0.7	4.5
Percentage of total voltage [%]	44.4	13.3	26.7	15.6	100
Field strength [kV/mm]	0.303	0.05	0.194	0.017	

5.10 Discussion of Results

The arc voltage extinction peaks for tests with and without the "self-blast" were compared for two different electrode dimensions, see Fig. 5.17 and 5.18. For both electrodes, the voltage increased with more than 1 kV by using the "self-blast" setup. This shows that the increased pressure gives far better breaking capability, since more arc energy is removed before CZ.

To assess the breaking capability, the shapes and values of the breaking currents can give good information. For both electrode dimensions, it was demonstrated that using the "self-blast" setup gave more favorable breaking currents. The peaks were higher and they oscillated more which indicates that the breaker is "more eager" to interrupt the current.

High post-arc currents increase the risk of re-ignitions. From the results, it was found that the "self-blast" setup gave much lower post-arc currents, for both electrode dimensions. The lower currents should result in a longer lifetime of the switch.

When investigating how the arc voltage distribution and field strength changes, from before CZ to after. For the test with the 4.0 mm electrode and without "self-blast", about 73 % of the arc voltage was across sections 3 and 4. The field strength in section 3, where the gas outlet was located, increased significantly after the CZ crossing, see Table 5.1 and 5.2.
This was also the case for the 6.0 mm electrode test, where 87.5 % of the arc voltage was across the last two sections, before and after CZ. The field strength also here increased greatly in section 3, see Table 5.3 and 5.4. This shows that the field strength across the gas outlet increases significantly after CZ. The placement of the gas outlet, thus has a large impact on the voltage distribution for the circuit breaker without "self-blast".

Using the "self-blast" setup with the 4.0 mm electrode, greatly altered how the voltage distribution changed from before to after CZ. Referring to Table 5.5 and 5.6, more than 60 % of the voltage was across section 4 before CZ. After CZ, almost 60 % of the arc voltage was distributed over sections 1 and 2. This also increased the field strength in all the sections, and it was now slightly higher in section 1 than in section 3. The field strength increased from 0.045 kV/mm before CZ to 0.273 kV/mm after, in section 1. The arc-current was also significantly lower after CZ, it dropped from 117 mA to 17 mA.

Using the 6.0 mm electrode gave similar results, referring to Table 5.7 and 5.8. The arc

voltage shifted from being mostly distributed over the two last sections before CZ, to the two first sections after CZ. Thus, having the same characteristic as the 4.0 mm electrode. The difference was though not as substantial as for the smaller electrode. The field strengths also in this case increased, and it increased in section 1 from 0.152 kV/mm before CZ to 0.303 kV after CZ. The current was again about 100 mA lower after CZ.

By comparing the voltage distribution after CZ, between the two electrode dimensions. The tests without the "self-blast" setup showed that the field strength was much higher in the section were the gas outlet was located, almost two times higher than in the other sections. In the test with 4.0 mm electrode, the field strength was 0.194 kV/mm and with the 6.0 mm electrode it was 0.113 kV/mm, as shown in Table 5.2 and 5.4.

Introducing the "self-blast" setup, greatly affected the voltage distribution after CZ for both electrode dimensions. In the first section, the field strengths were 0.273 kV/mm and 0.303 kV/mm for the 4.0 mm and 6.0 mm electrode respectively. In the section with the gas outlet it was 0.242 kV/mm for the 4.0 mm electrode and 0.194 kV/mm for the 6.0 mm electrode. It is evident, that the pressure inside the ablation tube strongly affects how the arc voltage is distributed after current interruption.

Chapter 6

Summary and Recommendations for Future Work

6.1 Summary and Conclusions

In this authors previous work [3], it was found that the measurements had certain flaws. The biggest concern was that the plotted voltage curves did not cross zero at the same instant in time. The first part of this thesis looked at its cause and suggested a solution.

Initially it was though that it was the Debye shielding effect, which occurs at the probe tip was the cause of this problem. In the Debye sheath, there will be a voltage drop. This voltage drop was calculated and used in both simulations and the actual measurements to see if it was the source of the problem. From this it was concluded that the voltage drop in the sheath was too small to be the sole reason for the measurement error.

The frequency response for one probe was also measured. From the measurement, it was concluded that the frequency response of the probe should be sufficient for the tests conducted in this work.

The reason behind the voltage shifts did not seem to be solely caused by the ones mentioned, another approach was therefore implemented. By using simple equations, a voltage correction was calculated. The voltage correction was calculated using the relation between resistance, capacitance and the voltage gradient. By applying this correction to the measurements from the laboratory work, the voltages now crossed zero at the same point in time.

To view the repeatability of laboratory setup, two identical breaking operations were conducted for each test. Based upon this it could be concluded that the tests were reproducible.

To state where the results are valid, the probe currents were calculated and compared to the current through the arc. It was found that the results are valid from contact separation and until 100 μs after current interruption.

From the results, the following main conclusions were drawn:

- From the work conducted in this report, it can be concluded that high voltage resistive probes can be used for conductivity measurement in switching arcs. This applies only if the measurements are corrected using a correction method and certain time interval, as described in this report.
- The voltage distribution and field strength for different sections of the arc were calculated. For the tests without the "self-blast" setup it was found that most of the voltage was distributed over the last two sections. The field strength increased significantly in the section containing the gas outlet, from 20 μs before CZ to 20 μs after. When using the "self-blast" setup, the increase was not as high.
- When using the "self-blast" setup, the voltage distribution shifted. From before CZ to after, the field strength increased immensely in the first section. Thus, the pressure has a great impact on the voltage distribution.
- Using the "self-blast" setup improved the current interruption capability of the circuit breaker significantly.

6.2 Recommendations for Future Work

- In this work, only one type of ablation material was used. Using other polymer materials could result in improved breaking capability. One suggestion is to use Polytetrafluoroethylene (PTFE), which is often used as ablation material in these types of breakers.
- From the measurements, it was clear that some unknown factors influenced the results. This most likely was caused by stray capacitances. These should be measured and the measurements should be corrected accordingly.
- It could be beneficial to develop a more detailed simulation model of the circuit. This could give valuable insight to how the test object is influenced by the measuring equipment. This could be done by measuring parameters of the physical setup and implementing them in a model. The model could be developed in programs like Simulink or ATPDraw, and using an arc model like a Cassie and Mayr arc-model.

- The probes could not measure voltages above ca. 5 kV, this can be solved by connecting the probes in series.

Appendix A

Simulink Model

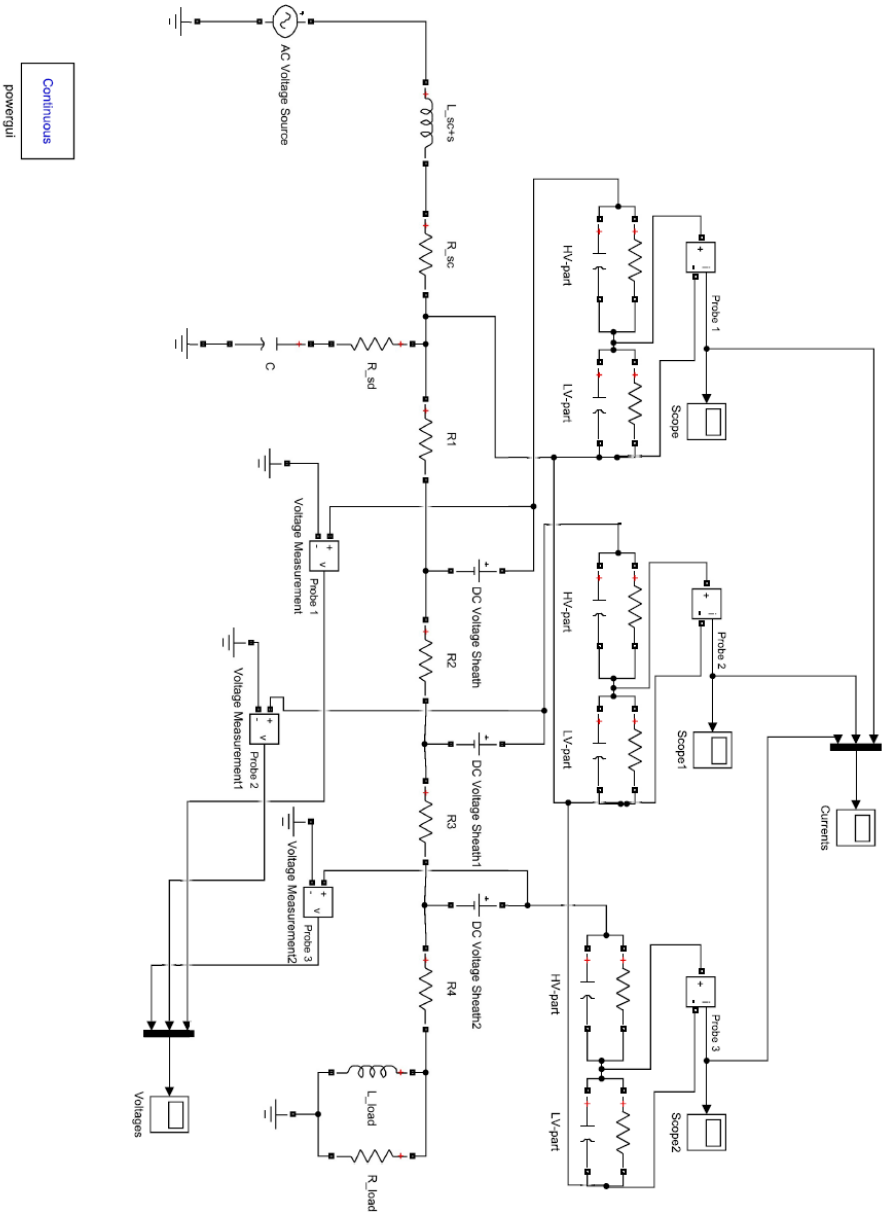

Figure A.1: The Simulink circuit used for testing the impact of Debye shielding.

Appendix B

Probe voltages at CZ crossing

Table B.1: The probe voltages when the voltage across the test object is 0 at CZ.

Test number	Probe 1 [kV]	Probe 2 [kV]	Probe 3 [kV]
507	-0.59	-0.03	-0.01
508	-0.06	-0.15	0.11
509	-0.03	-0.01	-0.02
510	0.03	-0.07	0.17
511	-0.11	-0.07	-0.14
512	0.03	-0.06	0.17
513	-0.12	-0.14	0.19
514	-0.17	-0.14	0.17
515	-0.09	0.33	0.14
516	-0.14	-0.07	-0.14
517	-0.04	0.47	0.23
518	0.26	1.16	-0.05
519	0.01	0.74	-0.11
520	-0.03	0.06	-0.28
521	-0.10	0.03	-0.19
522	-0.09	0.037	-0.21
523	-0.09	0.03	-0.19

Bibliography

[1] M. Keidar. *Plasma Engineering: Applications from Aerospace to Bio and Nanotechnology*. Elsevier Science.

[2] F. F. Chen. Langmuir probe diagnostics. *Langmuir probe*, 2003.

[3] T. R. Settendal. Specialization project, conductivity measurement in switching arcs, 2016.

[4] M. Runde. *Current Interruption in Power Grids*. NTNU, 2015.

[5] I. H. Hutchinson. *Principles of plasma diagnostics*. Cambridge University Press, 2nd ed. edition.

[6] H. Taxt. Ablation-assisted current interruption in medium voltage switchgear – development and prospect. *24th Nordic Insulation Symposium on Materials, Components and Diagnostics (NORDIS-15); 2015-06-15 - 2015-06-17 NTNU*, 2015.

[7] H. Taxt, M. Runde, K. Niayesh, and E. Jonsson. Experimental investigation on ablation-assisted current interruption - experimental setup and preliminary results. *post-arc-current, ablation, medium voltage, load-break switch*, 2016.

[8] R. L. Merlino. Understanding langmuir probe current-voltage characteristics. 75(12):1078–1085.

[9] Reduced-mass. https://en.wikipedia.org/w/index.php?title=Reduced_mass&oldid=763770100.

[10] F. F. Chen. Thickness of combined bohm-langmuir sheaths. *Langmuir probe*, 1979.

[11] Low pass filter - passive RC filter tutorial, 2013. http://www.electronics-tutorials.ws/filter/filter_2.html.

[12] A. Ahmethodzic, M. Kapetanovic, K. Sokolija, R. P. P. Smeets, and V. Kertesz. Linking a physical arc model with a black box arc model and verification. 18(4):1029–1037.

[13] H. M. Looe, J. D. Yan, and J. W. Spencer. Development of a non-SF6 self-blast type interrupter unit. In *2008 17th International Conference on Gas Discharges and Their Applications*, pages 117–120.